Geophysical Fluid Dynamics: from the Lab, up and down!

Henri-Claude Nataf
Univ Grenoble Alpes / CNRS
Grenoble, France

Fluid Dynamics in Earth and Planetary Sciences
Kyoto, November 27-30, 2018

Lecture 2

Mantle convection and plate tectonics

FDEPS

Kyoto, November 27, 2018

outline

2.1. The blinding evidence for plate tectonics

The many signatures of plate tectonics today

- a survey of geophysical observables compiled at http://jules.unavco.org/Voyager/Earth

topography - bathymetry

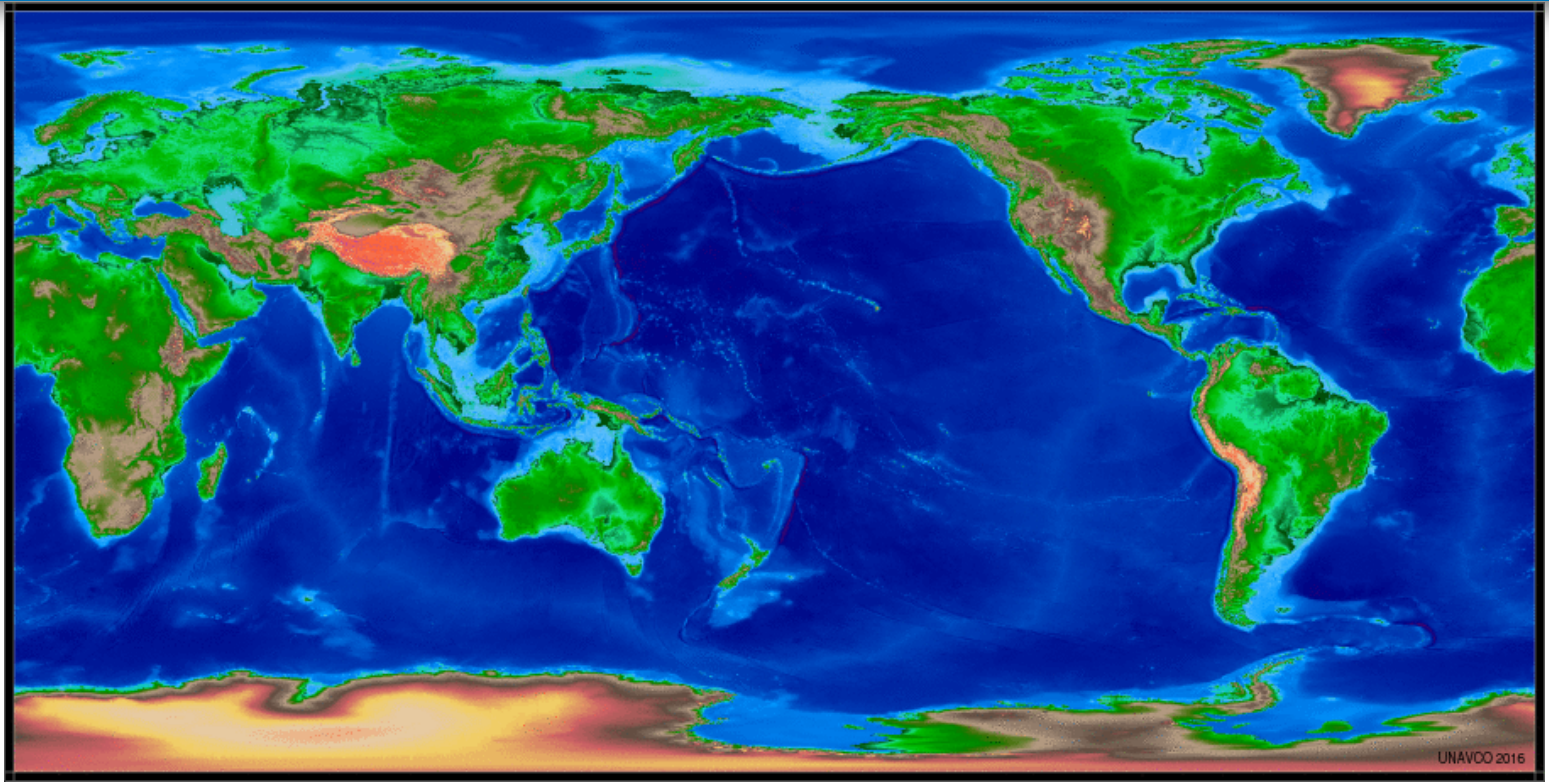

free air gravity anomalies

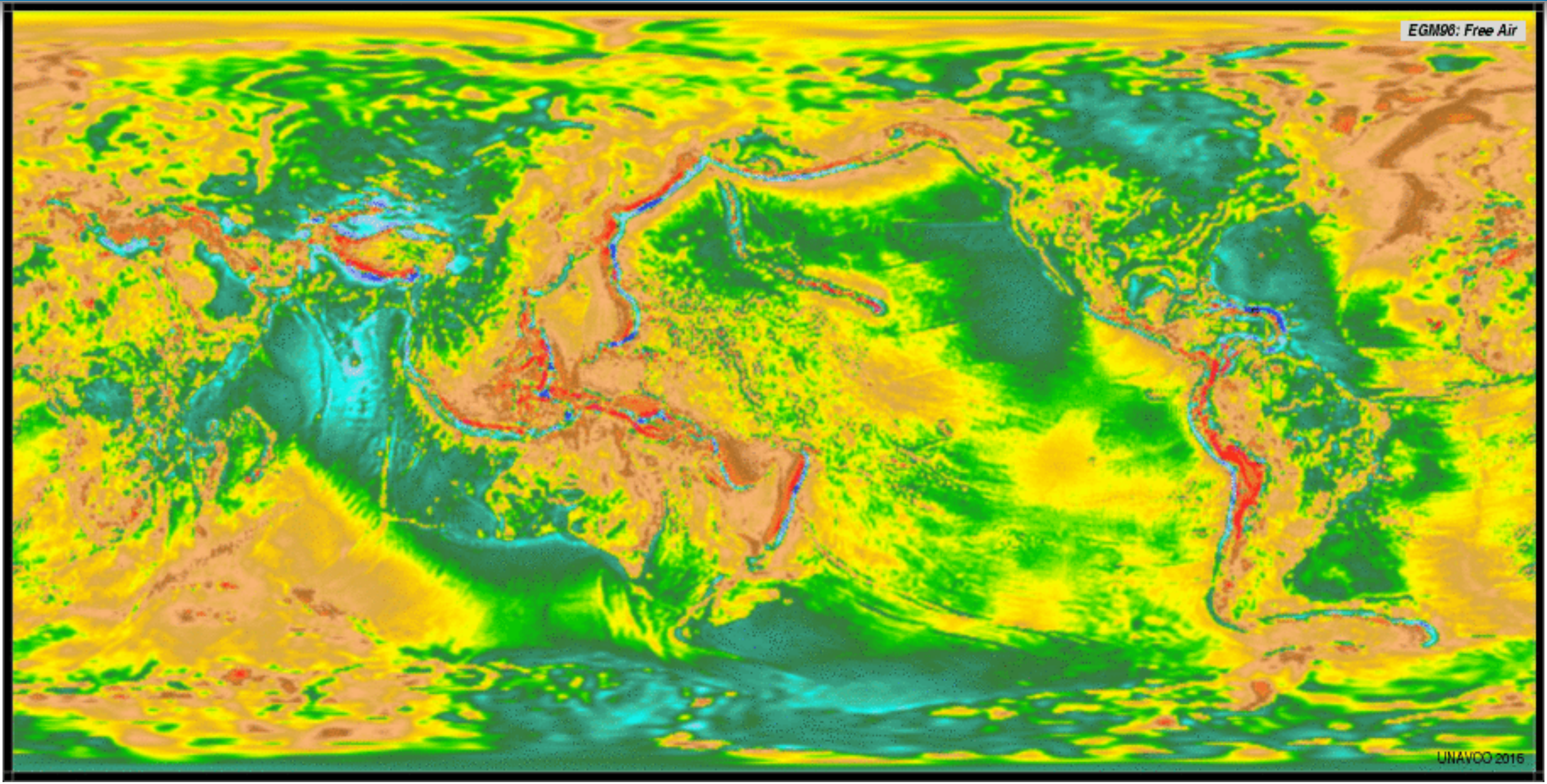

seismicity

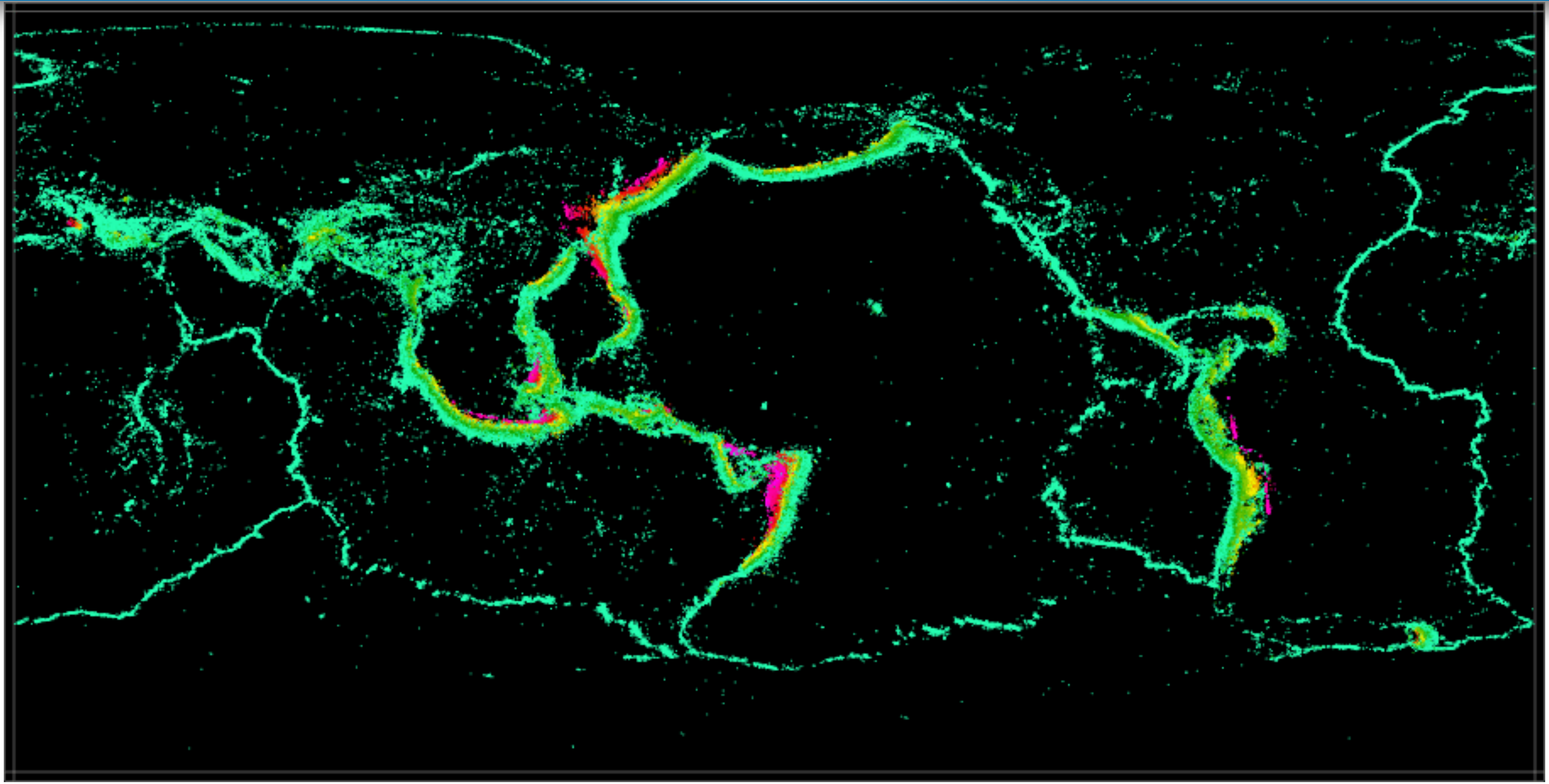

earthquake focal mechanisms

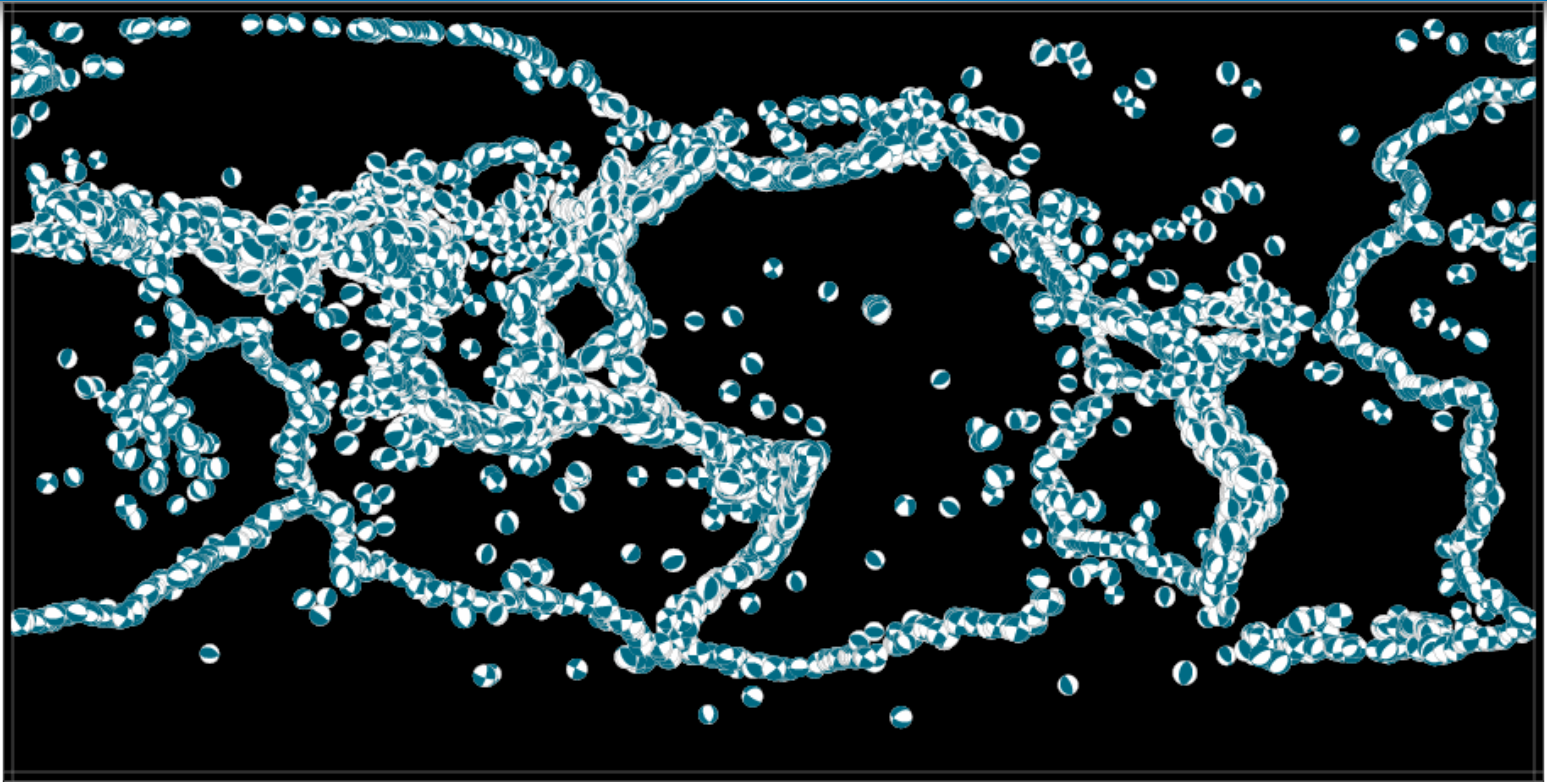

stresses

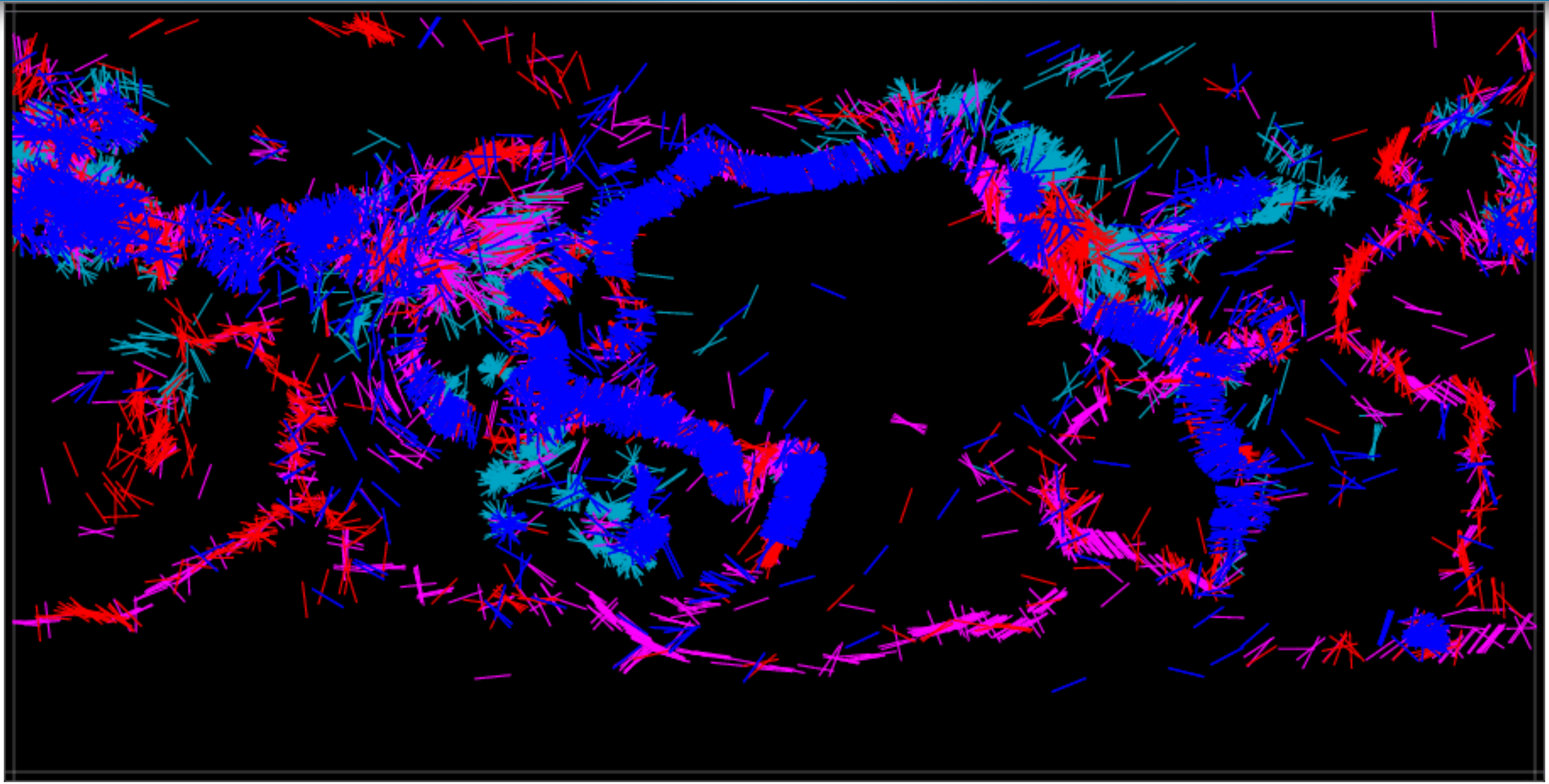

oceanic floor age

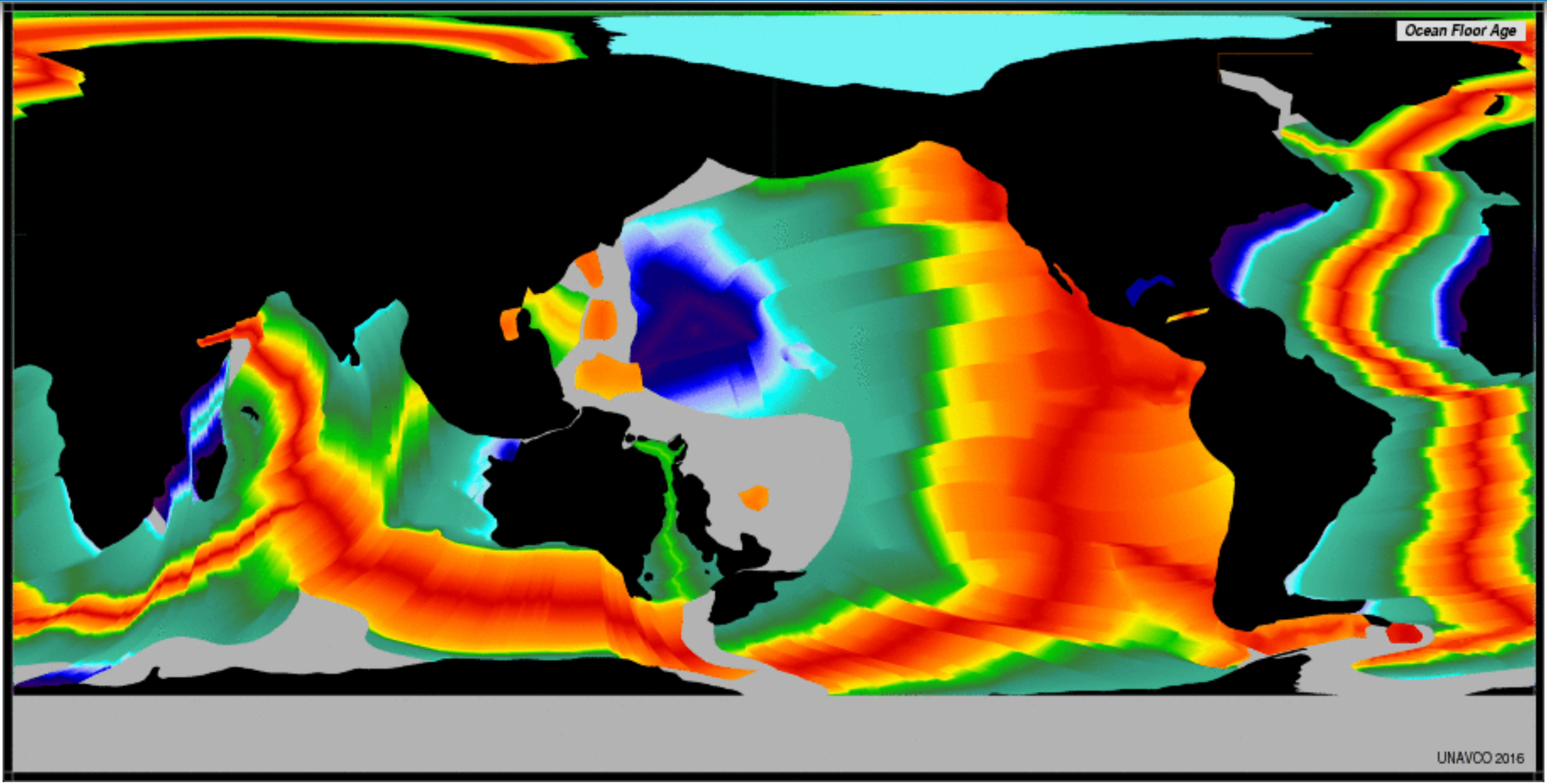

GPS velocities

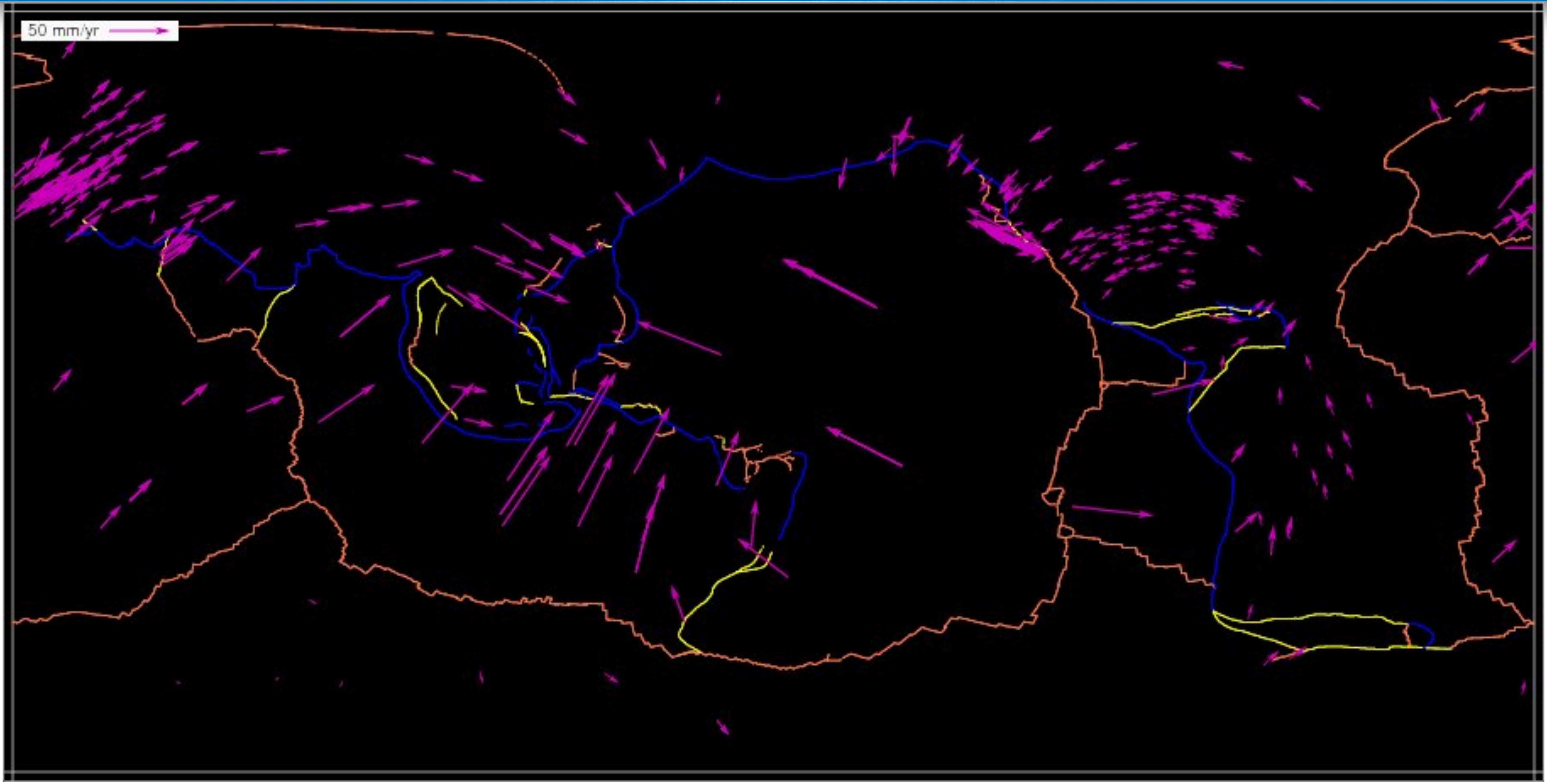

Holocene active volcanoes

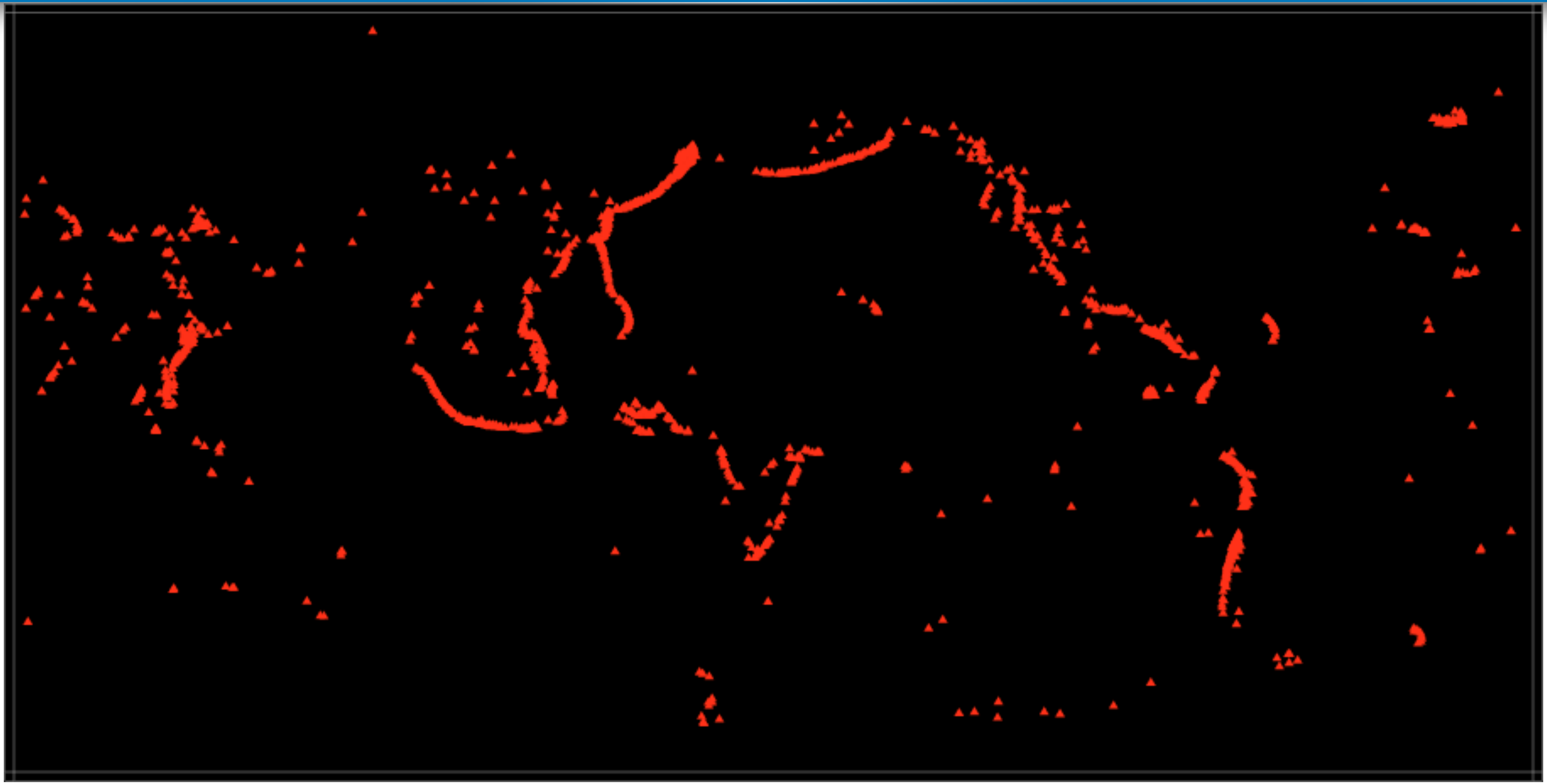

Figure captions for reference

Topography

R G B	meters
214 214 214	8622
191 064 153	6000
255 101 056	5000
241 159 115	4200
232 204 165	3700
242 207 099	3200
206 098 102	2700
096 078 065	2200
140 120 105	1700
183 157 132	1200
060 110 000	800
000 131 000	600
000 149 000	400
000 189 000	200
028 227 148	100
000 070 000	0
000 205 193	-1
057 193 193	-20
098 193 255	-40
049 172 255	-80
000 151 255	-200
000 130 238	-400
000 109 220	-800
000 088 203	-1600
000 068 186	-2800
000 047 169	-4000
000 005 134	-6000
080 000 112	-8000
000 065 086	-10644

Free-air gravity anomalies

R G B	milligal
202 043 255	485
237 137 239	400
242 134 183	300
232 023 117	200
255 000 000	150
255 109 052	100
242 136 040	80
170 108 040	60
255 185 121	40
218 171 063	20
254 203 001	10
255 255 000	0
000 202 000	-10
055 123 058	-20
051 147 120	-40
065 190 156	-60
000 255 255	-80
169 237 237	-100
151 151 255	-150
000 000 255	-200
000 000 072	-331

Seismicity

R G B	km
038 255 179	<=33
000 166 000	50
124 197 000	120
255 255 000	200
234 129 000	300
234 000 000	400
255 000 127	500
255 000 255	670
227 177 255	750

Stresses

R G B	eigenvalues	(deformation)
000 000 000	e2 = e1 > 0	(pure anti-divergence)
255 255 255	e2 = e1 > 0	(pure anti-divergence)
000 000 255	e2 = 0, e1 > 0	(pure compression)
000 255 255	2*e2 = -e1, e1 > 0	
000 194 000	e2 = -e1	(pure shear)
255 255 000	2*e1 = -e2, e2 < 0	
255 000 000	e1 = 0, e2 < 0	(pure tension)
255 000 255	e1 = e2 < 0	(pure divergence)

Oceanic floor age

ocean floor age in Myr (millions of years before present day)

R G B	Myr
210 000 000	0
245 045 000	10.9
255 098 000	20.1
255 148 000	33.1
255 198 000	40.1
248 242 000	47.9
000 202 000	55.9
055 123 058	67.7
051 147 120	83.5
065 190 156	120.4
000 255 255	126.7
169 237 237	131.9
151 151 255	139.6
000 000 255	147.7
000 000 125	154.3
094 000 094	180

a zoom on Japan and Kamchatka

Topography

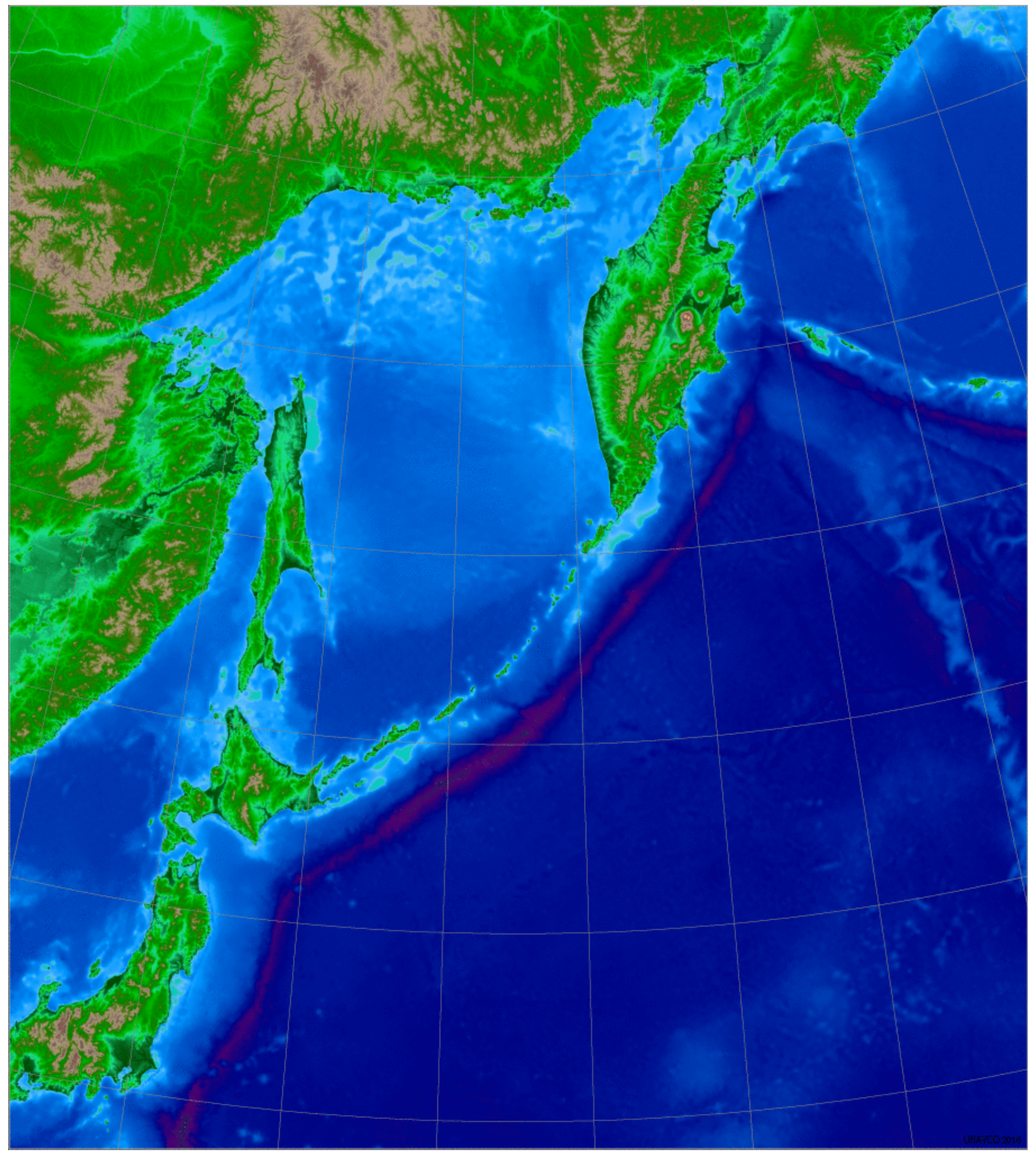

Free-air gravity

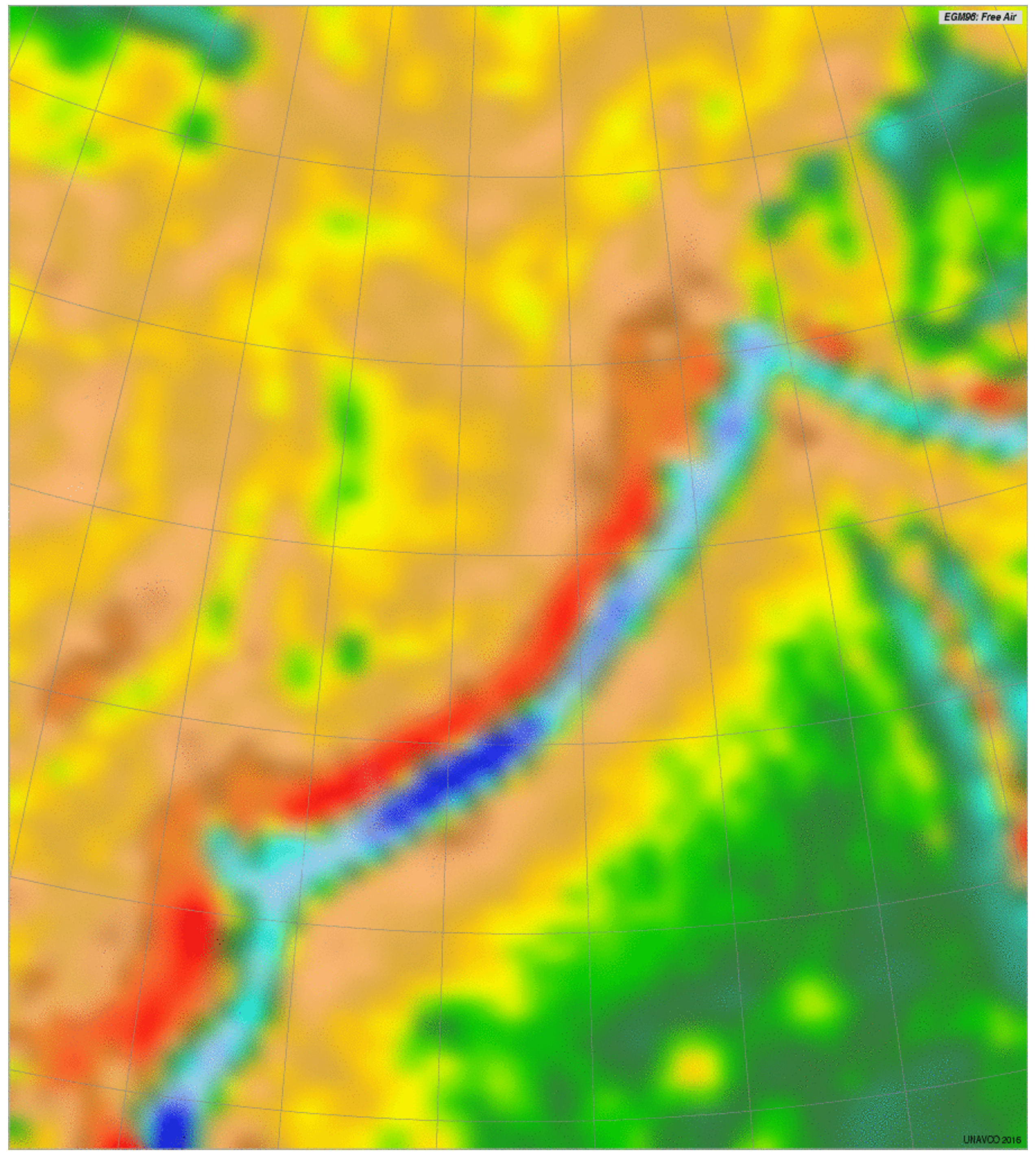

Seismicity

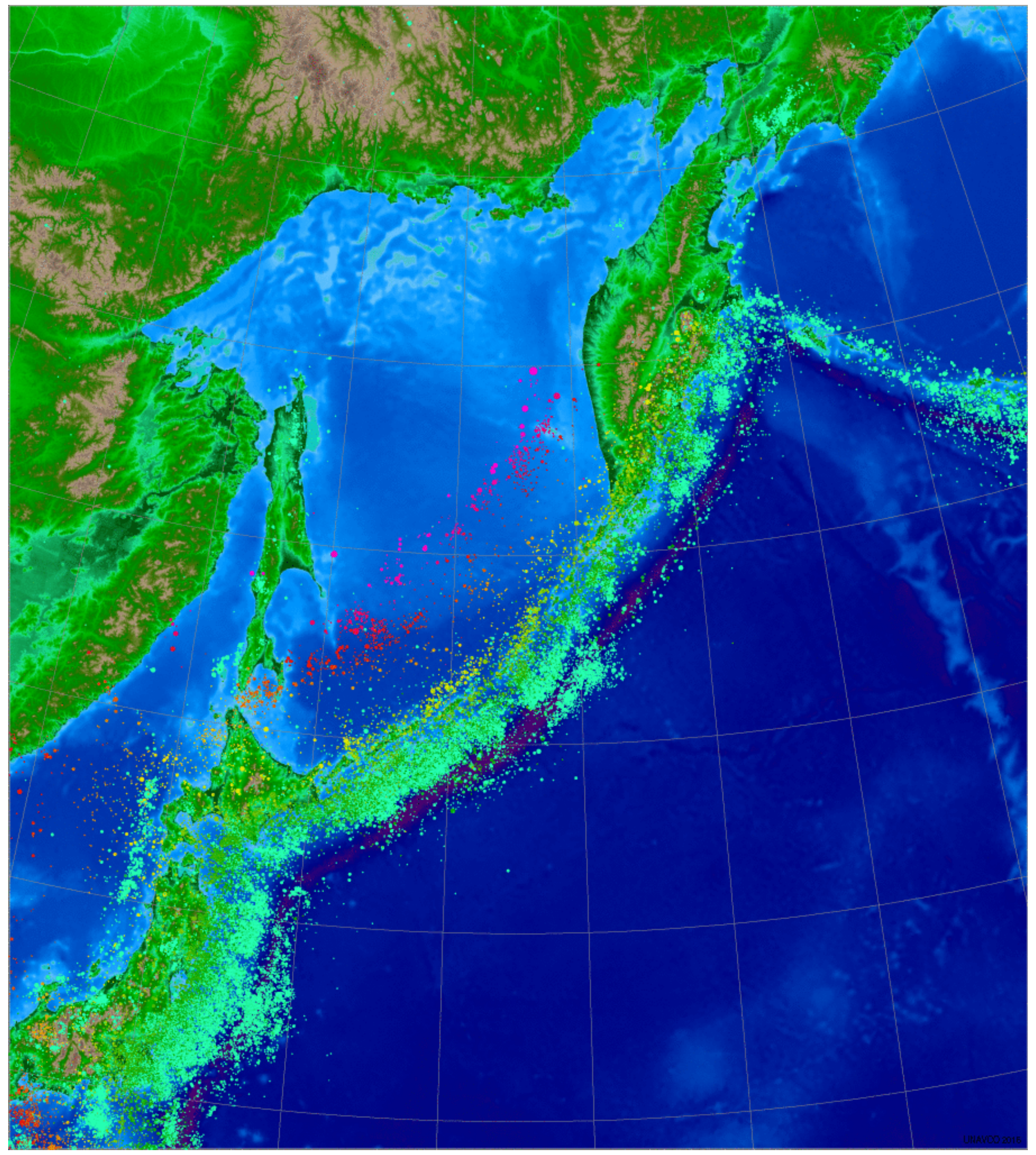

focal mechanisms

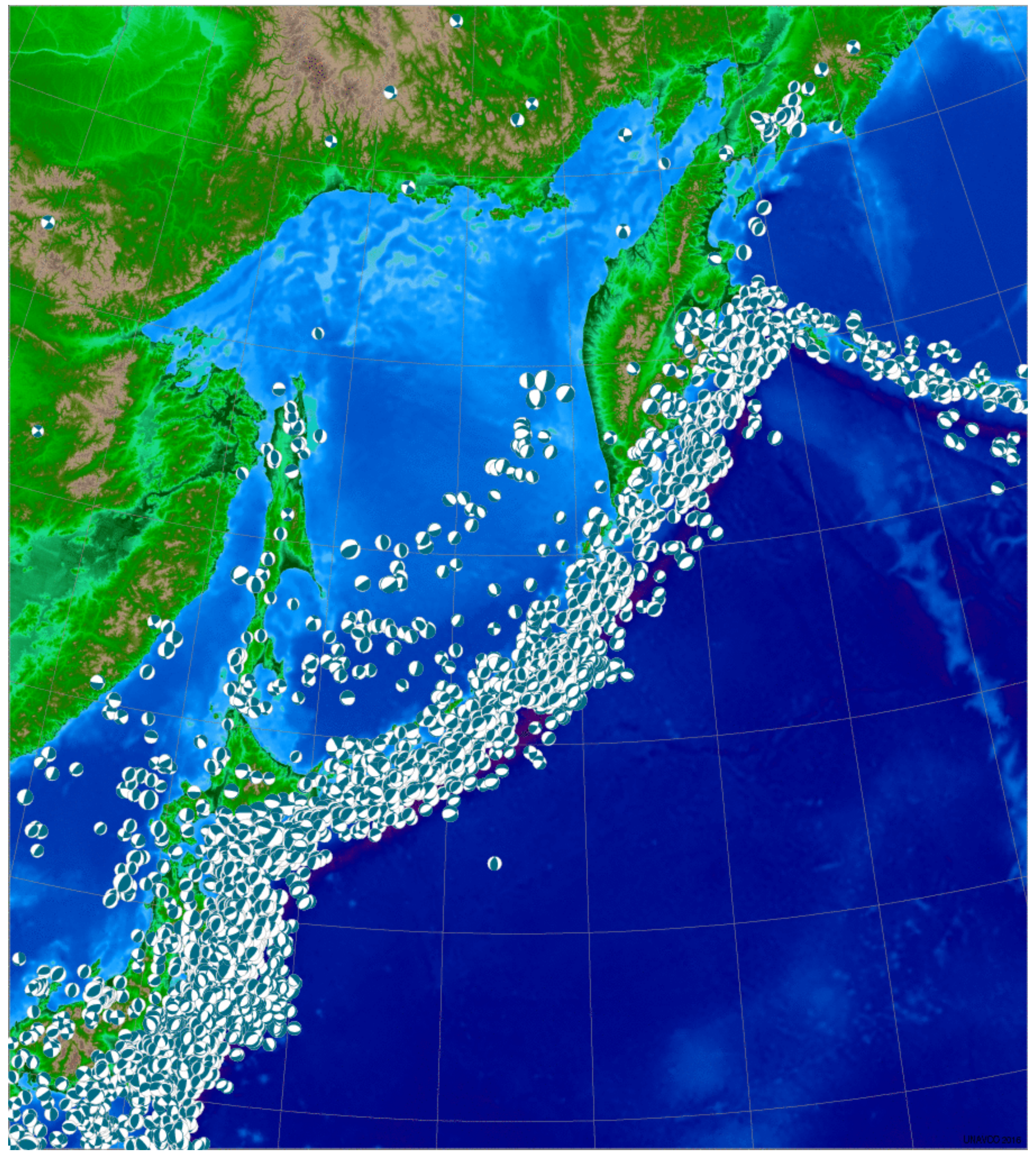

Questions…

- What happens to plates sinking into the mantle?
- What is the origin of hotspots?
- How does subduction initiate?
- When did plate tectonics begin?
- Why is it not seen on other planets?

2.2. Mantle convection with T-dependent viscosity

T-dependent viscosity

- The viscosity of the constituents of the mantle varies strongly with temperature. The viscosity of the **cold lithosphere** is several orders of magnitude larger than the viscosity of the **hot asthenosphere**.

- What are the consequences of this fundamental property of mantle convection?

- Let's look at a very simple problem: the linear stability of Rayleigh-Bénard convection in a fluid with a viscosity ν varying with temperature T as:
  $\nu(T) = \nu_b \, e^{-\gamma(T_b - T)}$
- One can solve the linear stability of this (non-Boussinesq) problem, but we first look at it with heuristic arguments.

A simple convection problem

- Considering the sketch we have seen this morning, we start from the conductive solution. Therefore the temperature dependence of viscosity becomes a depth dependence: $\nu(z) = \nu_b \, e^{\gamma \Delta T \frac{z}{d}}$

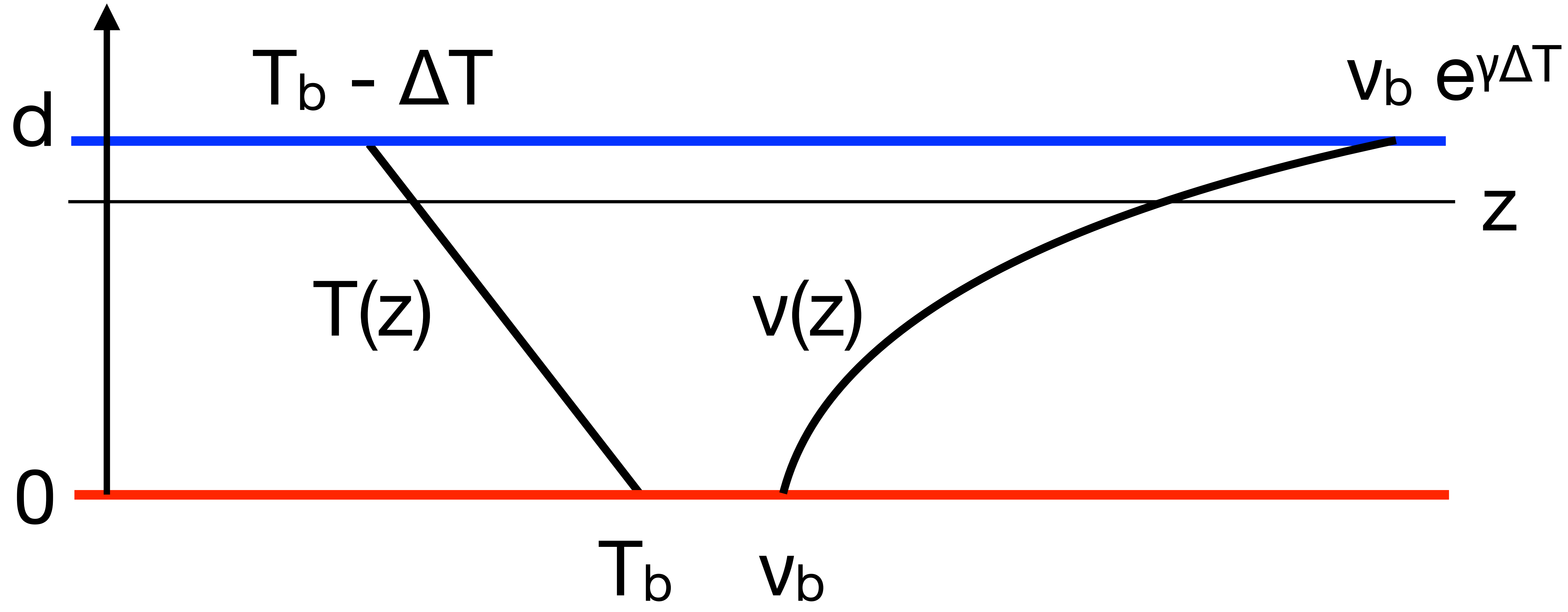

- Can convection develop in a sublayer between *0* and *z*, where viscosity is lower than at *d*?

Convection in a sublayer

- Let's compute the Rayleigh number Ra_z of this sublayer, picking the viscosity at mid-height as its 'representative viscosity':

$$\nu(z/2) = \nu_b e^{\gamma \Delta T \frac{z}{2d}}$$

Let's define: $Ra_b = \dfrac{\alpha \Delta T g d^3}{\kappa \nu_b}$ $\qquad r_\nu = e^{\gamma \Delta T}$ $\qquad \tilde{z} = \dfrac{z}{d}$

Then: $Ra_z = Ra_b\, \tilde{z}^4\, e^{\frac{\tilde{z}}{2} \ln r_\nu}$, which reaches a maximum for $\tilde{z}_m = \dfrac{8}{\ln r_\nu}$ ***if***

$$\ln r_\nu \geq 8 \iff r_\nu \geq e^8 = 2981$$

The viscosity ratio across this sublayer is always $e^8 = 2981$.

Critical Rayleigh number with T-dependent viscosity

- Indeed, if we compute the actual critical Rayleigh number Ra_c (still defined using viscosity at mid-height) as a function of viscosity ratio r_ν, we get:

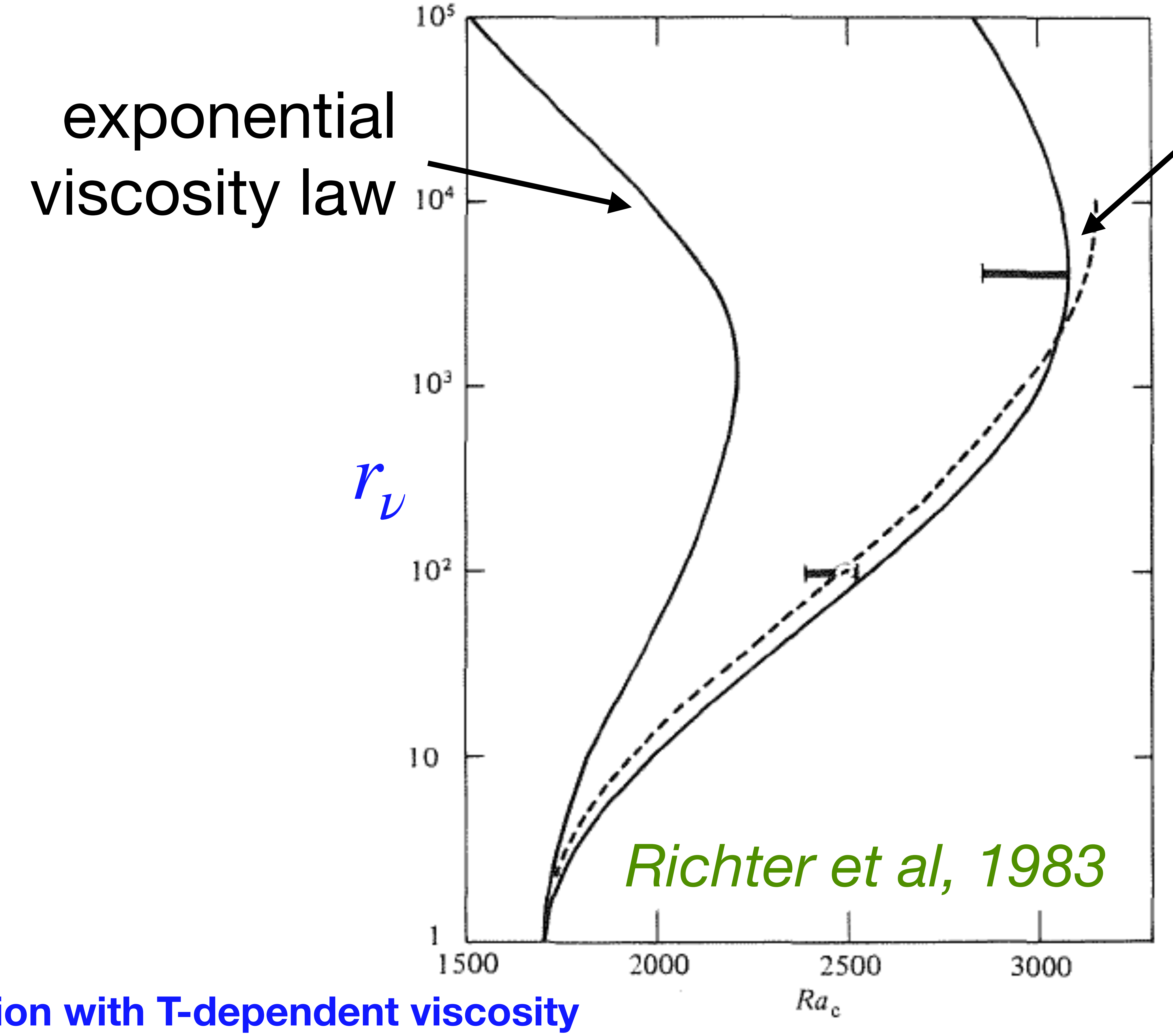

also: Stengel et al, 1982

Stagnant lid

- Once convection is restricted to a lower sublayer, the top part acts as an **motionless conductive lid**. Therefore, if we have the convection solution for the sublayer, we can easily **extrapolate** to the whole layer, and to any larger layer but by adding more viscous material at the top:

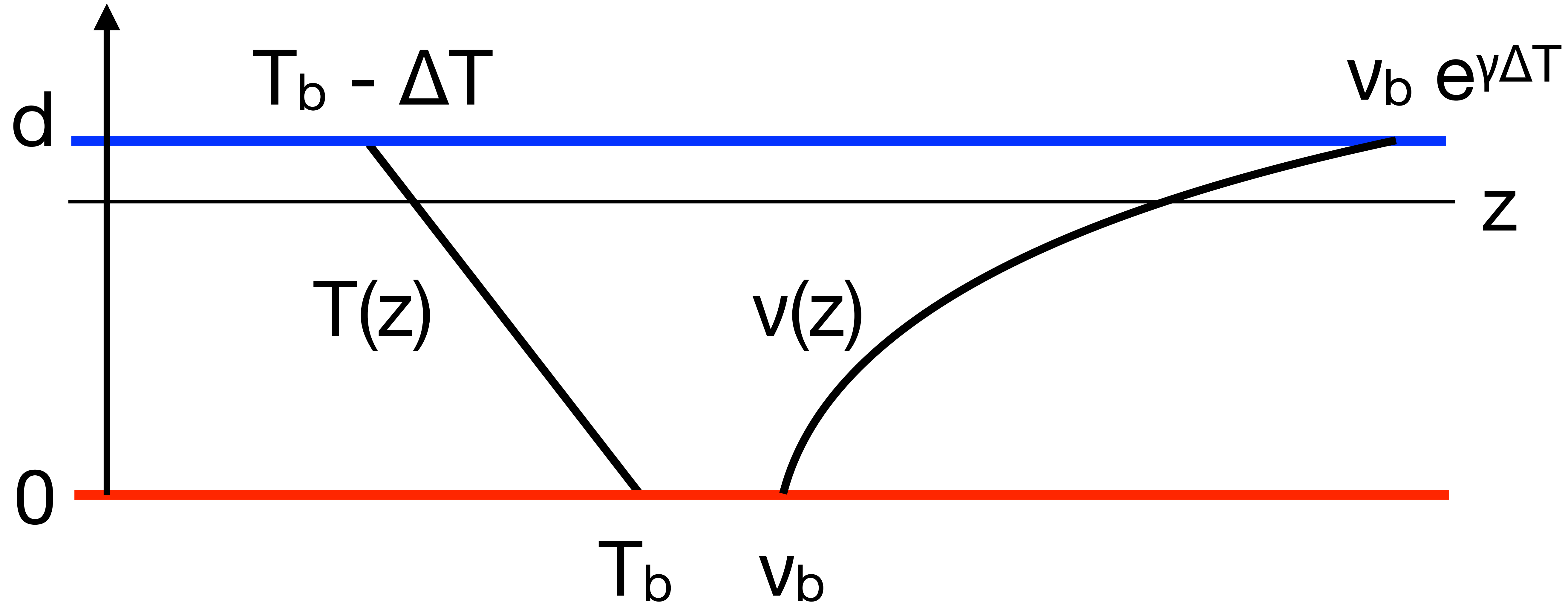

Stagnant lid at the convection threshold

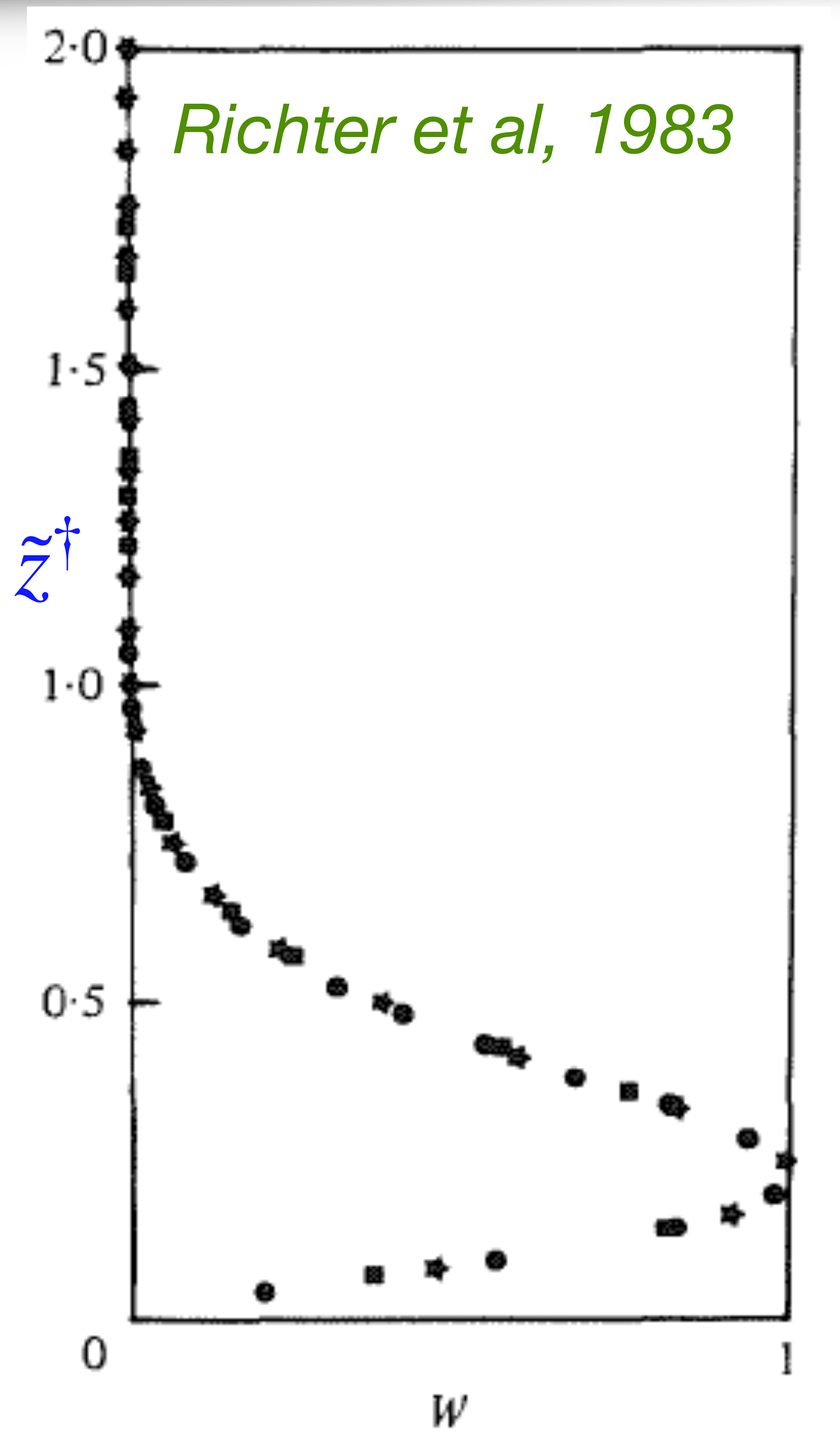

- This works well indeed, as demonstrated by the velocity eigenfunctions for linear instability at 3 different viscosity ratios (10^4, 10^6 and 10^8), plotted using a stretched coordinate

$$\tilde{z}^{\dagger} = \tilde{z}\frac{\ln r_{\nu}}{8}$$

Stagnant lid for developed convection

- The advantage of this approach is that can be generalized to other viscosity laws and to developed convection, focusing on the **horizontally-averaged temperature profile**.

Measuring horizontally-averaged temperature profiles

- Measuring the **horizontally-averaged temperature profile** in actual laboratory experiments:

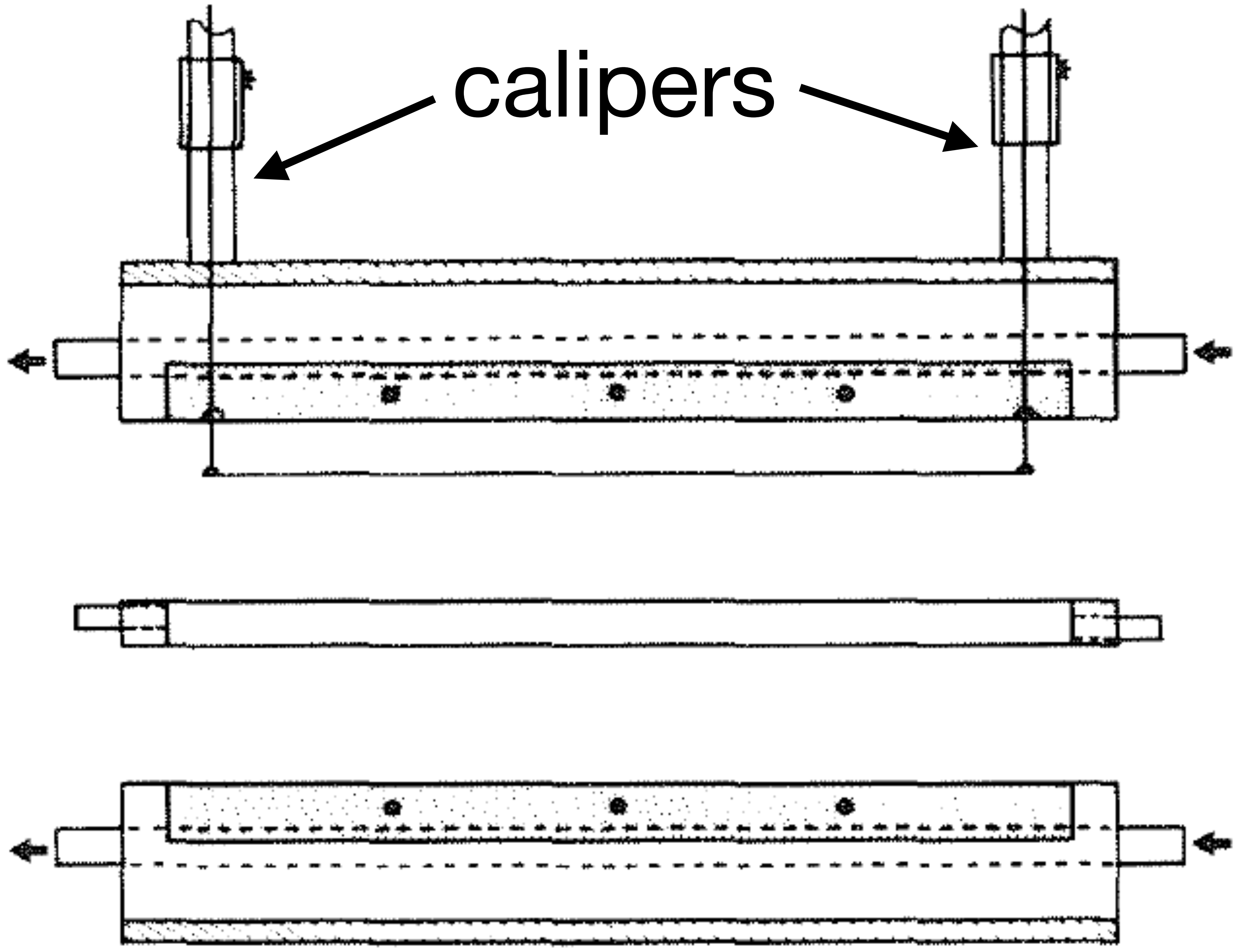

side view

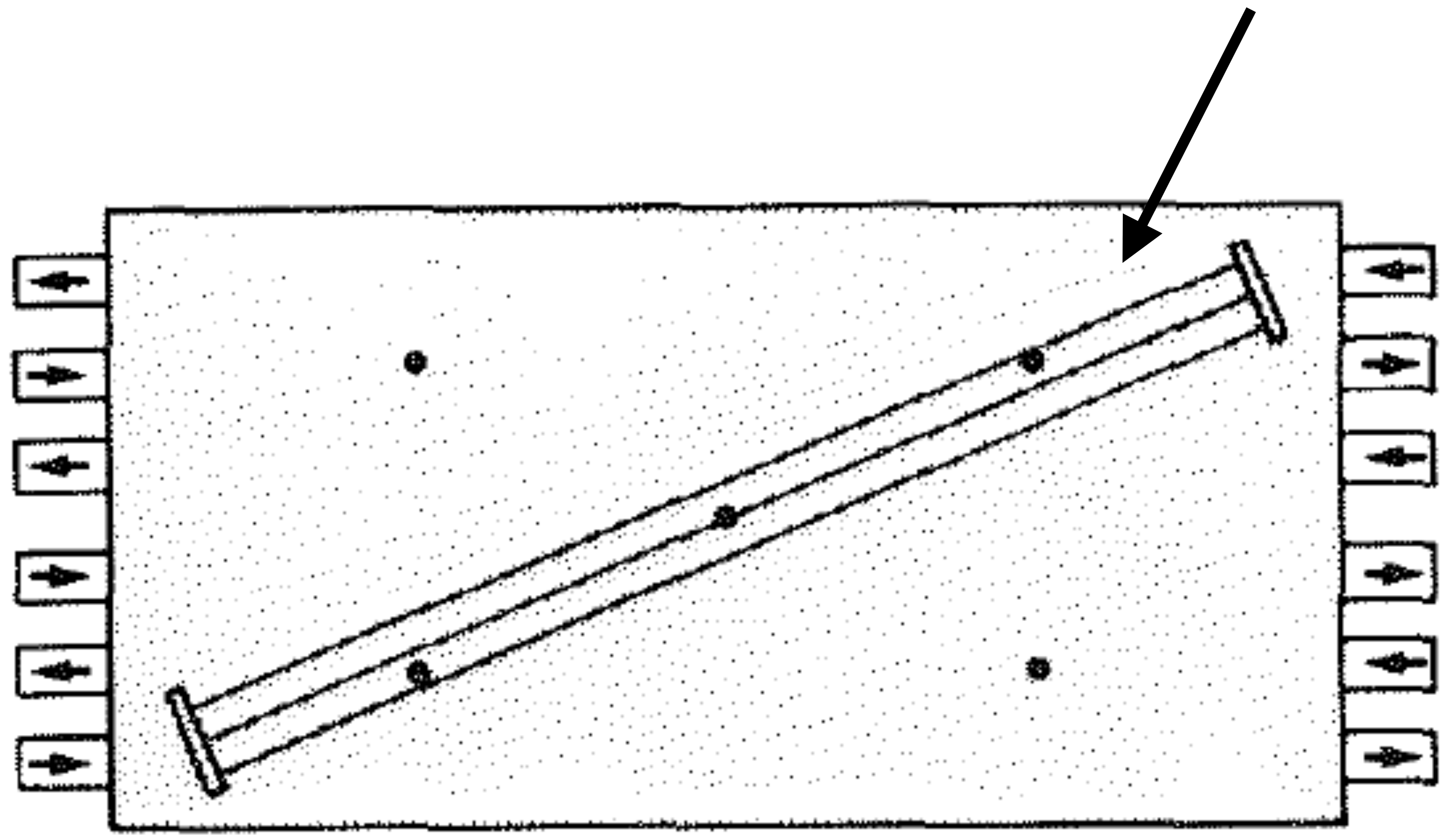

bottom view of the top plate

Richter et al, 1983

The offset of interior temperature in Laboratory experiments

- Experimental horizontally-averaged temperature profiles with $Ra_{1/2} \sim 10^5$, and three different viscosity ratios:

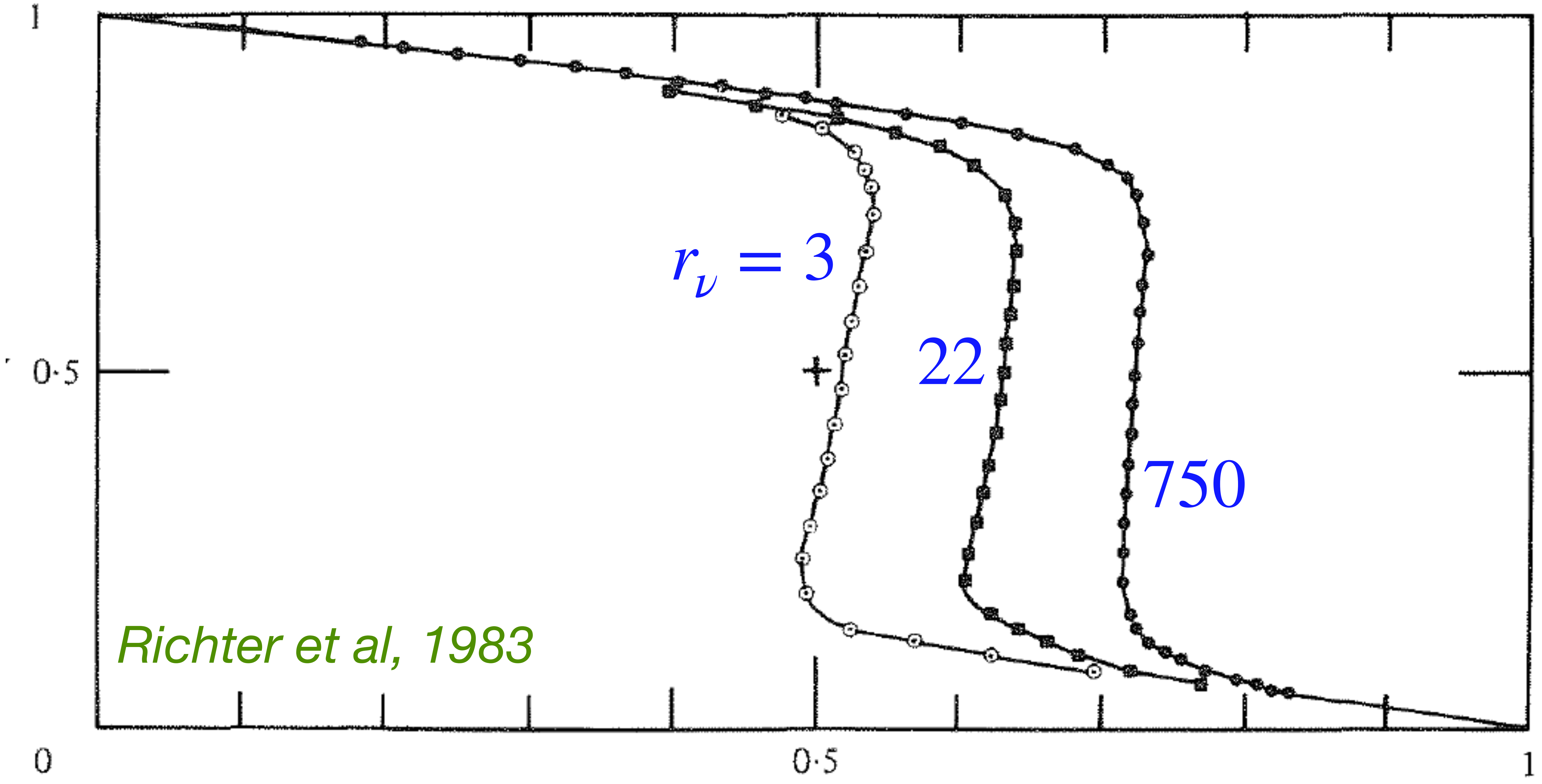

Two remarks

- Two important conclusions:

1) Mantle convection beneath a **stagnant lid** is really what we expect and it seems that this situation prevails for most planets (+ volcanism). Unless the lid viscosity is low enough to allow for convective motions.

2) The **viscosity ratio across the lower boundary layer** is self-limited to values of the order of **10 only**.

2.3. The mantle plume paradox

Hotspots

- Plates don’t get it all: intra-plate ‘**hotspot**’ volcanism appears to be an additional key component of mantle dynamics.

- As pointed out by Wilson (1961), they appear to correspond to heat sources that do not move while plates pass above them.

- Hawaii is the best known hotspot, and the track it left on the Pacific plate is impressive.

The Hawaiian hotspot track

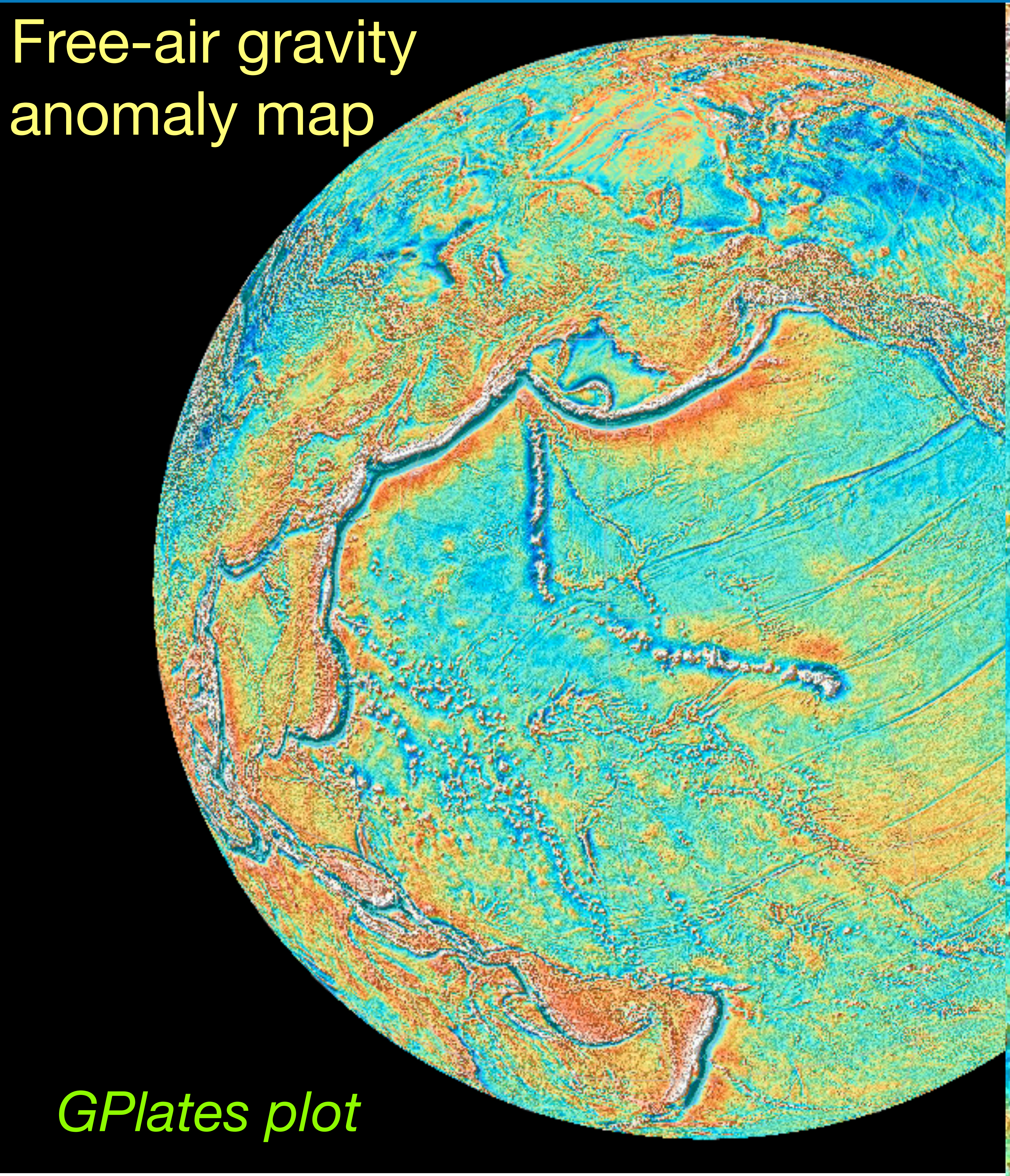

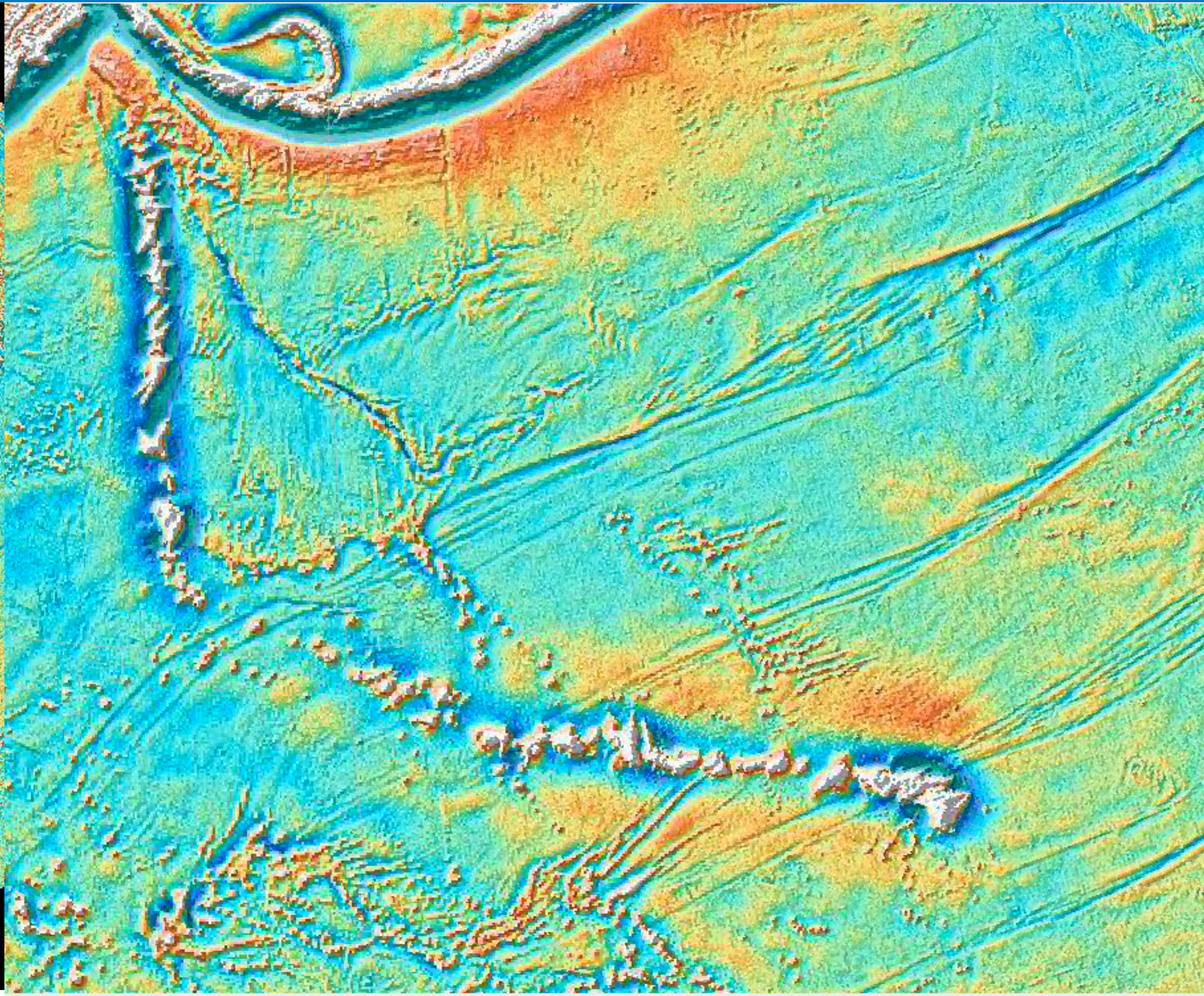

Geophysical and geochemical signatures of hotspots

- Hawaii is the best known hotspot, but geophysicists and geochemists have identified many more hotspots.

Radiogenic signatures of hotspots.

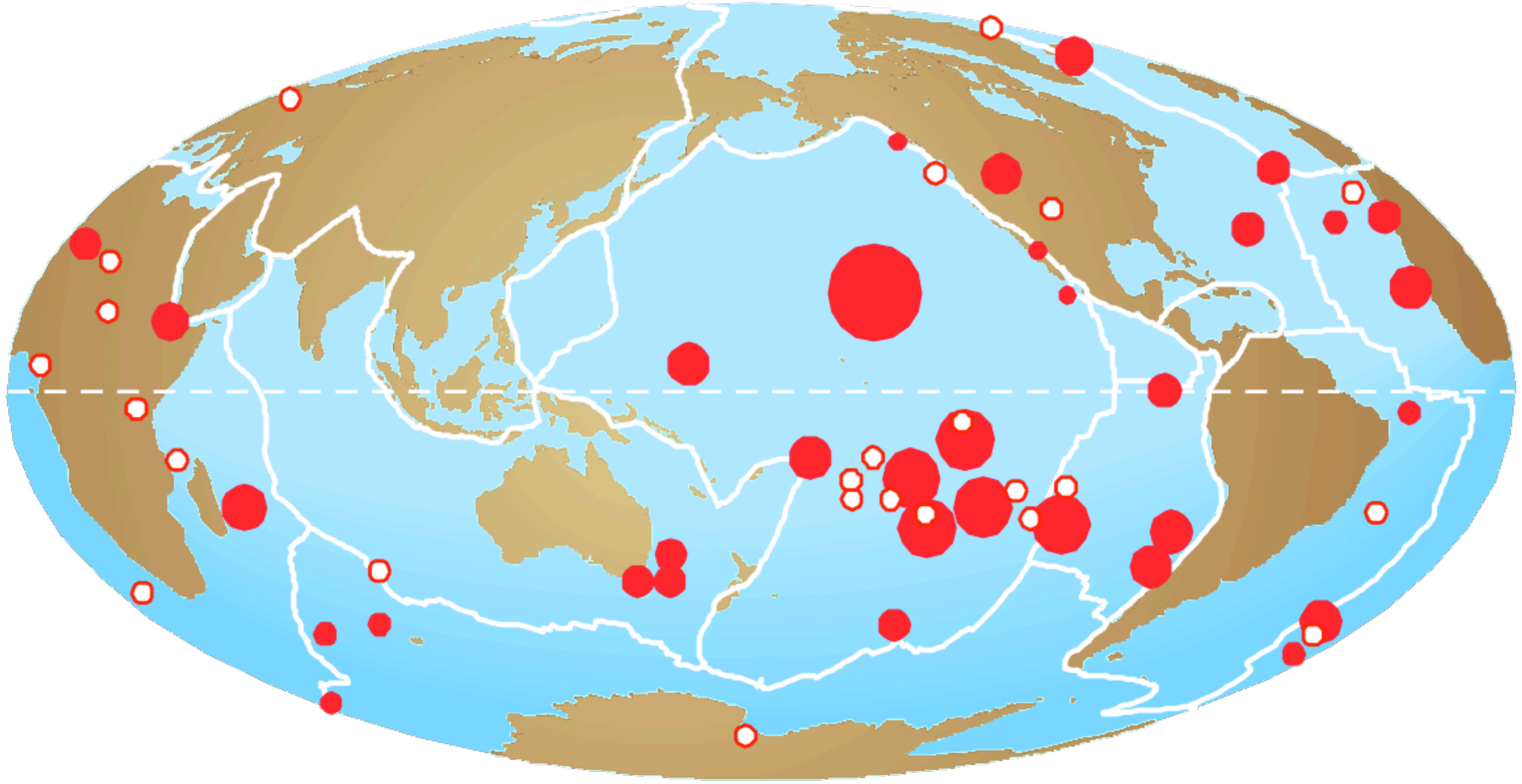

Buoyancy flux of hotspots, determined from the swell they produce beneath the lithosphere.

from Sleep, 1990

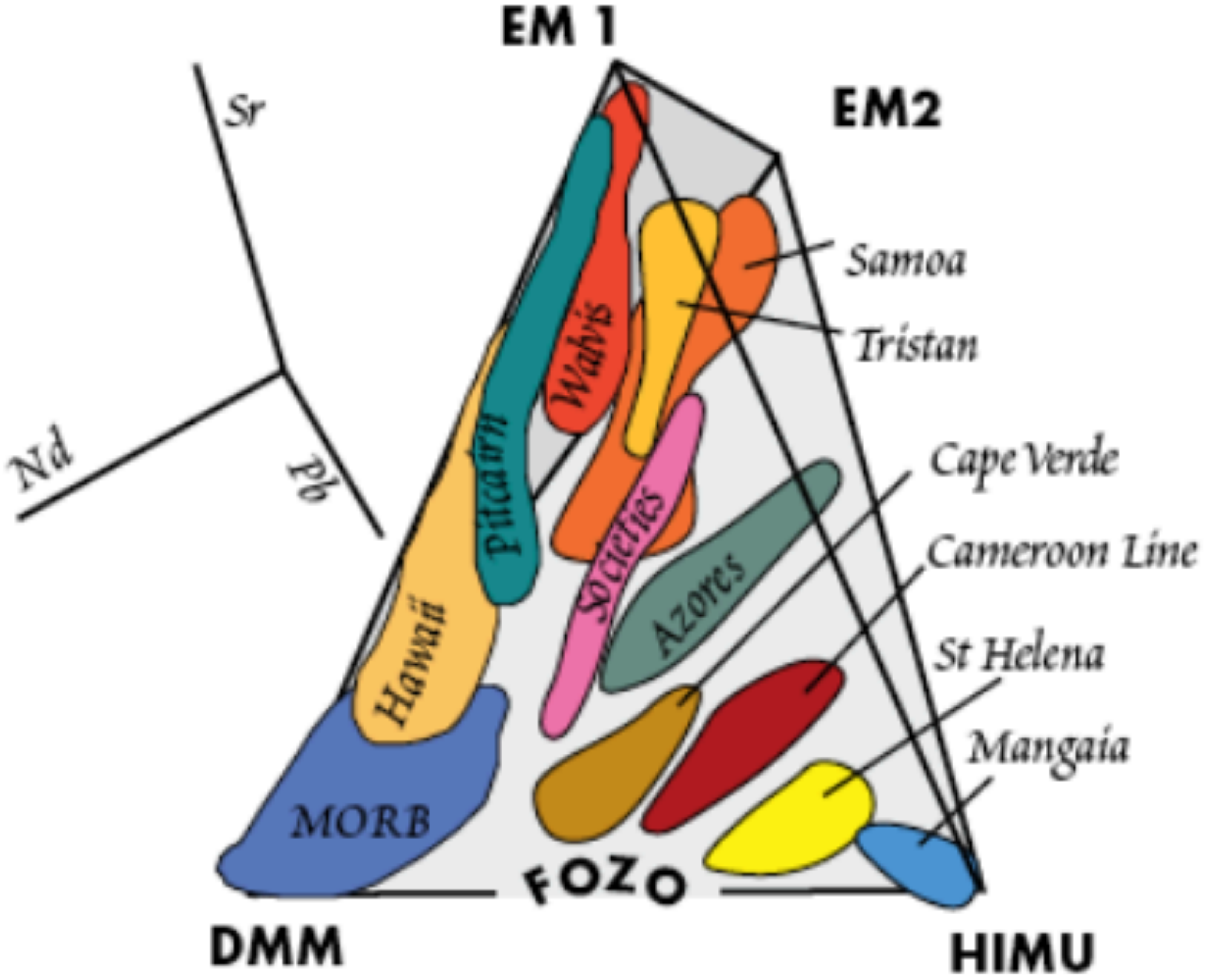

Figure 10.30. Three dimension plot of $^{87}Sr/^{86}Sr$, $^{143}Nd/^{144}Nd$, and $^{206}Pb/^{204}Pb$. Most oceanic basalt data plot within a tetrahedron defined by the composition of EMI, EMII, HIMU, and DMM components. Oceanic islands and island chains tend to form elongate isotopic arrays, many of which seem to point toward a focal zone (FOZO) at the base of the tetrahedron. Adapted from Hart et al. (1992).

Jason Morgan's mantle plume model

- The prevailing explanation is the '**mantle plume**' model of Morgan (1972), in which some hot plume originates from a boundary layer deep in the mantle, where convective velocities would be much slower than plate velocities.

- An additional clue comes from noting that the eruption of several **large igneous provinces (LIP)** coincide with the start of a hotspot track, and often also to the breaking of the overriding plate.

- A well known example is the La Réunion hotspot whose birth seems to date back to the Cretaceous-Tertiary boundary (65 Ma ago), when the huge Dekkan Traps were emplaced.

Dekkan Traps and La Réunion hotspot

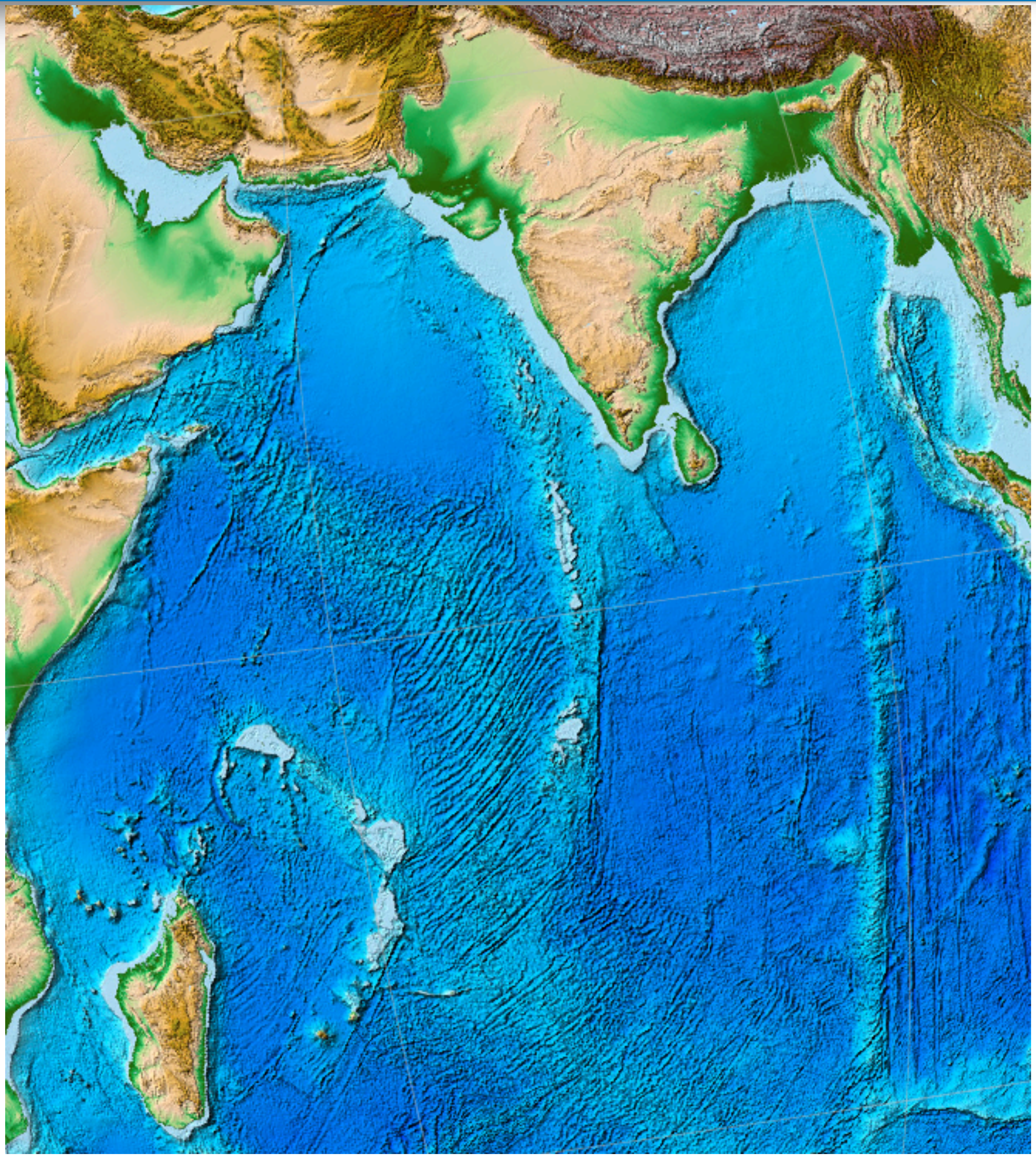

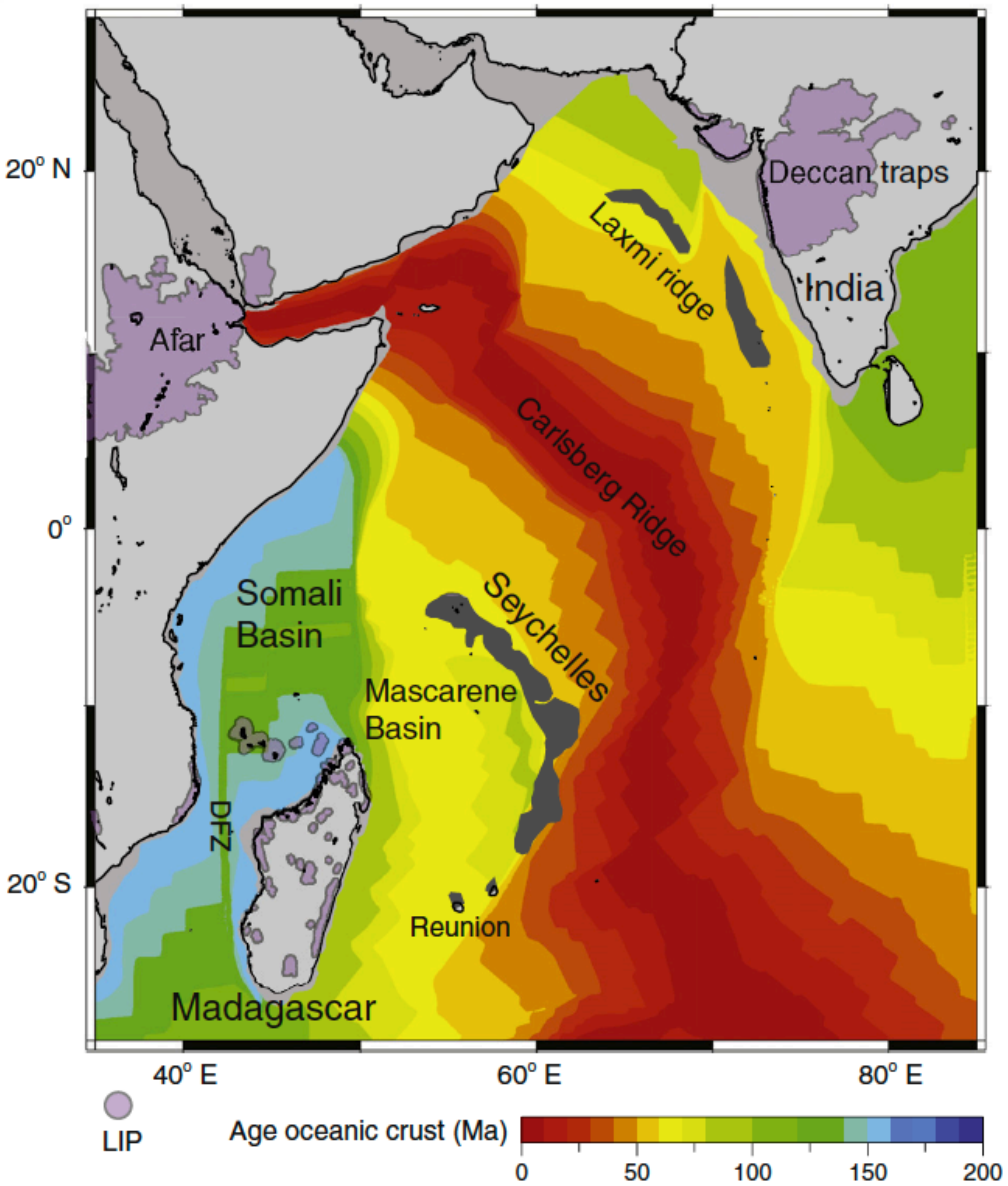

Buiter & Torsvik, 2014

Cavity plume

- This prompted the idea that mantle plumes could be **thermal cavity plumes** with a large temperature-dependent viscosity ratio, characterized by a **large head** fed by a **narrow tail** (Courtillot et al, 1986; Richards et al, 1989; Griffiths & Campbell, 1990).

- Experiments indeed show this behaviour when the hot injected fluid is some **100 times less viscous** than its surrounding.

The mantle plume paradox 1

- The viscosity ratio required to build thermal cavity plumes with a large head and a narrow tail appears to be **one order of magnitude larger** than the viscosity ratio built by T-dependent convection across its lower boundary layer.

- How can we solve this paradox?

Possible solutions to the mantle plume paradox

(1) Because of plate tectonics, some oceanic crust is returned to the mantle and accumulates at its base. It contains more heat-producing radioactive isotopes than the surrounding mantle. Therefore, it heats up gradually, and after a time of the order of a billion years, it forms a large buoyant plume.

This scenario, put forward by Hofmann & White (1982) also explains some geochemical properties of hotspot lavas.

Possible solutions to the mantle plume paradox

(2) Because of plate tectonics, the cold **subducting slab spreads** above the hot bottom, thereby increasing the temperature drop and viscosity ratio across the lower boundary layer.

This shows up (partly) in the experimental horizontally-average temperature profile of T-dependent convection with a moving upper lid.

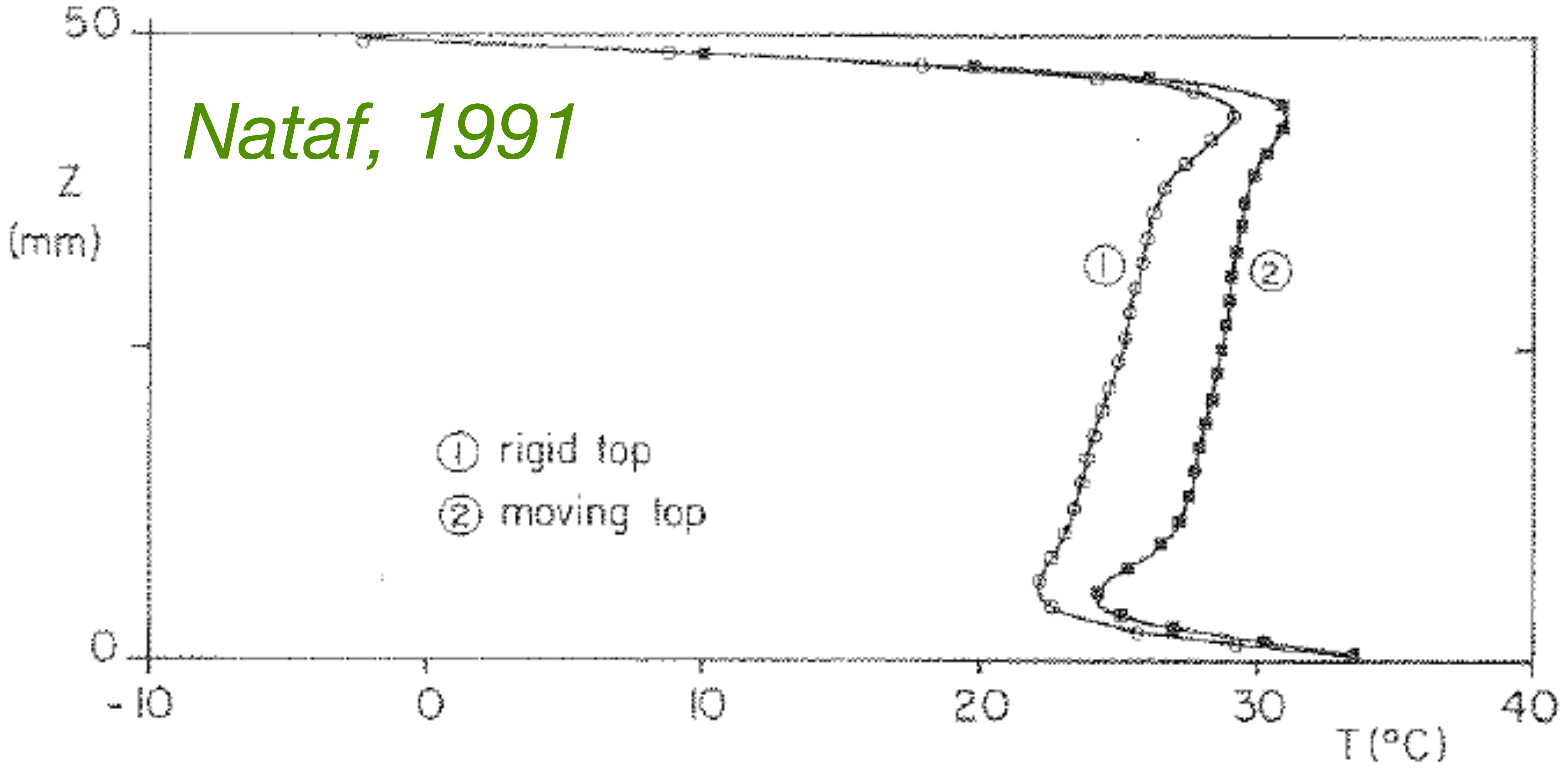

Fig. 5. Preliminary vertical profiles of horizontally averaged temperature. The overall viscosity variation is 100. Profile 1 is with a fixed rigid top boundary. Profile 2 was obtained with a moving top boundary that forced subduction. The velocity of the lid is approximately five times less than the maximum convective velocity. Note the lower temperature above the bottom boundary in profile 2. The shift towards high temperature at mid-depth for profile 2 is a bias of the averaging procedure. It disappears for larger velocities and/or larger viscosity ratios.

(3) A **dense layer** at the base of the mantle is entrained by a thermal plume. Depending on the density and viscosity ratios, plumes can take different styles.

In the experiments of Kumagai et al (2008), the fluid contains **thermochromic liquid crystals**, which mark the positions of isotherms.

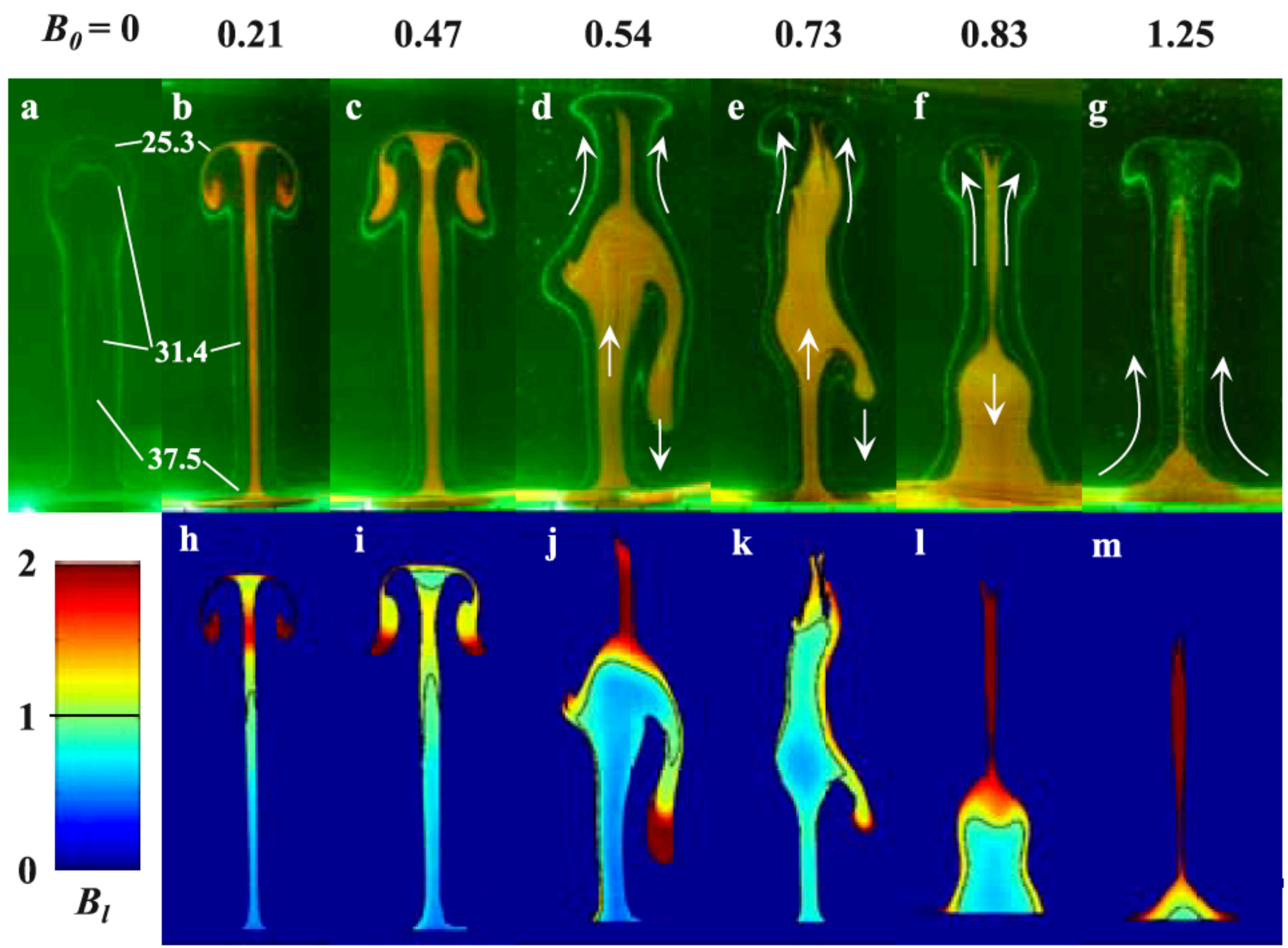

Kumagai et al, 2008

2.4. Seismic tomography

Seismic tomography

Ancestors' global models of the upper mantle...

a

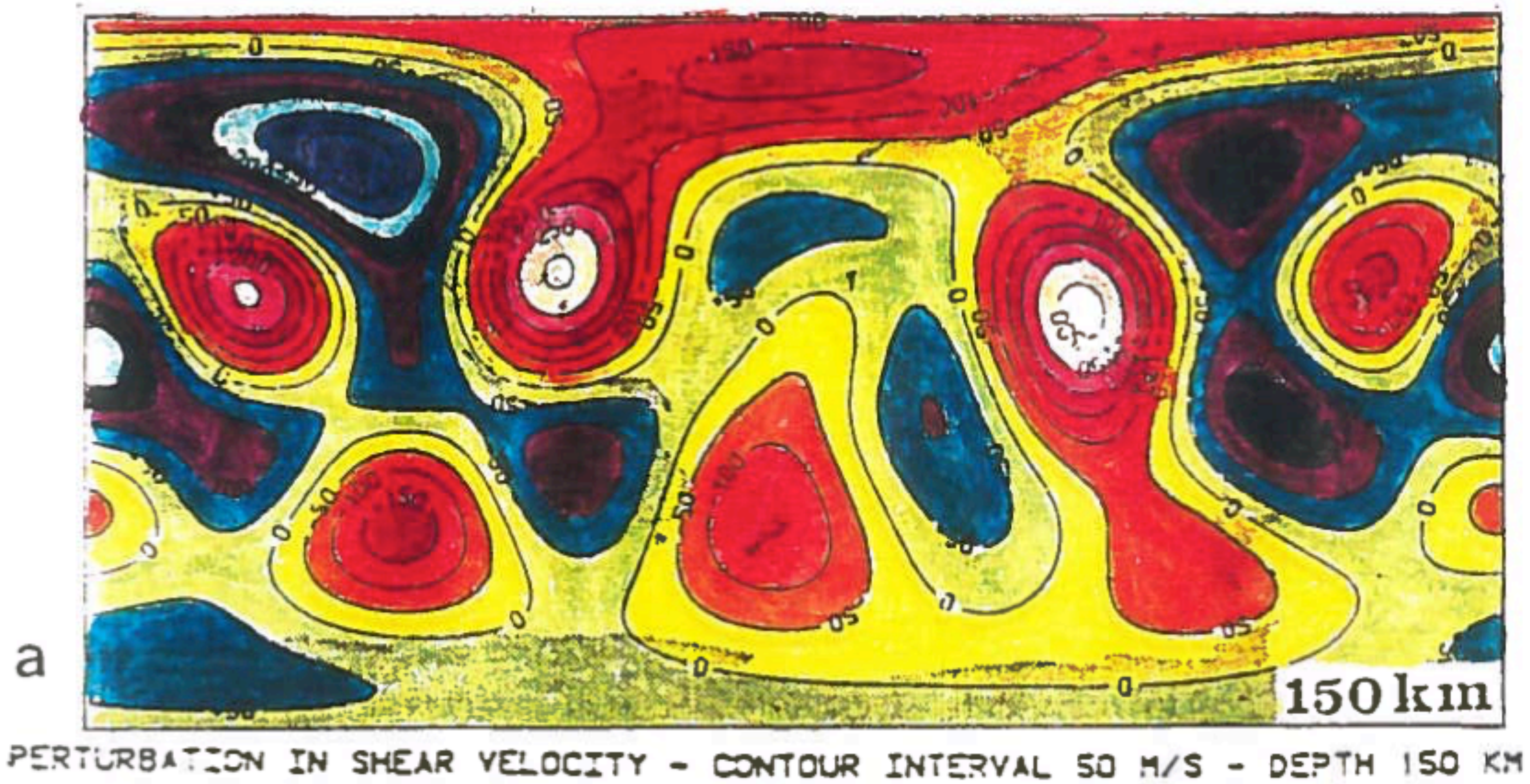

Nataf, Nakanishi & Anderson, 1984

a

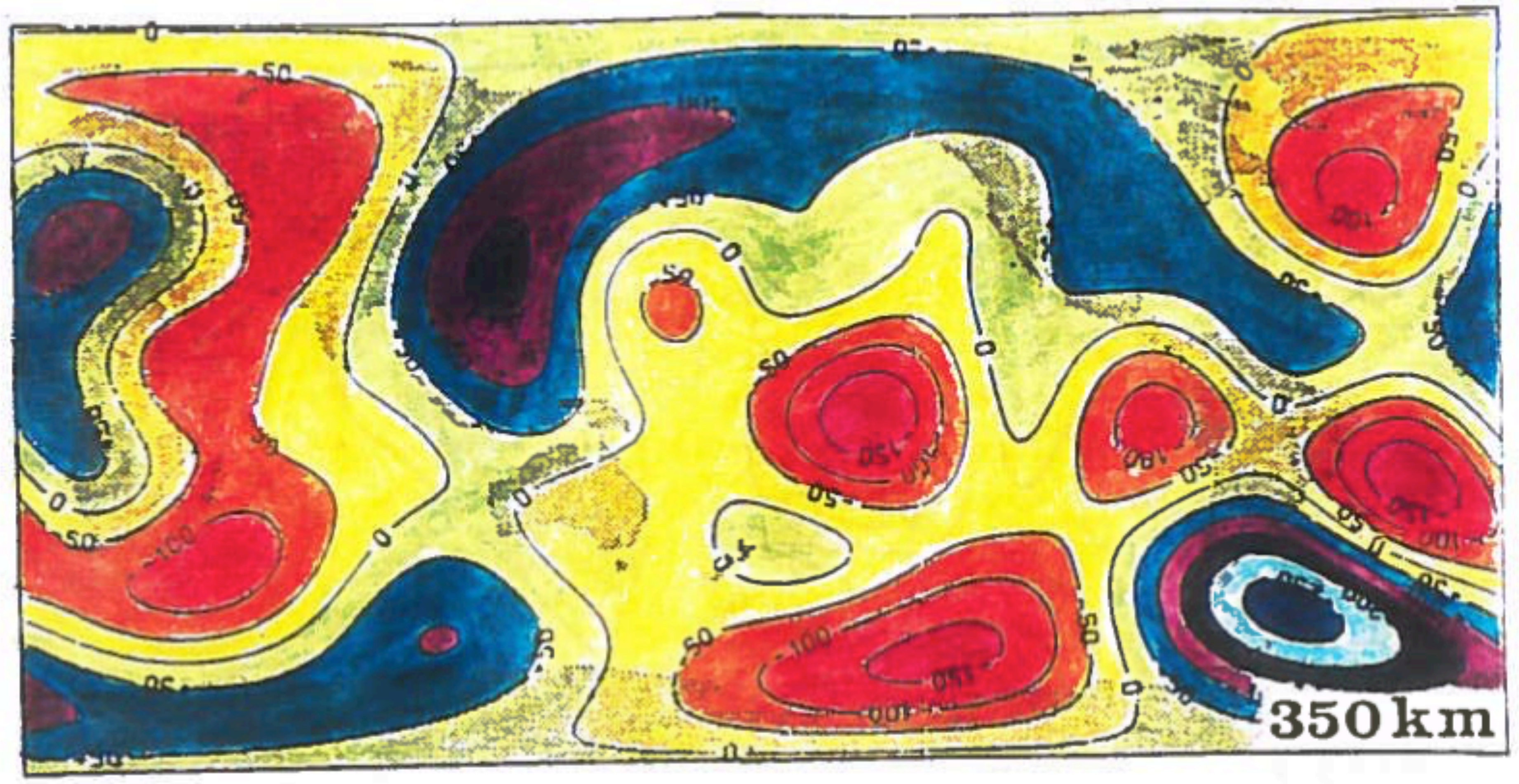

from 250 fundamental Rayleigh + Love waves

b

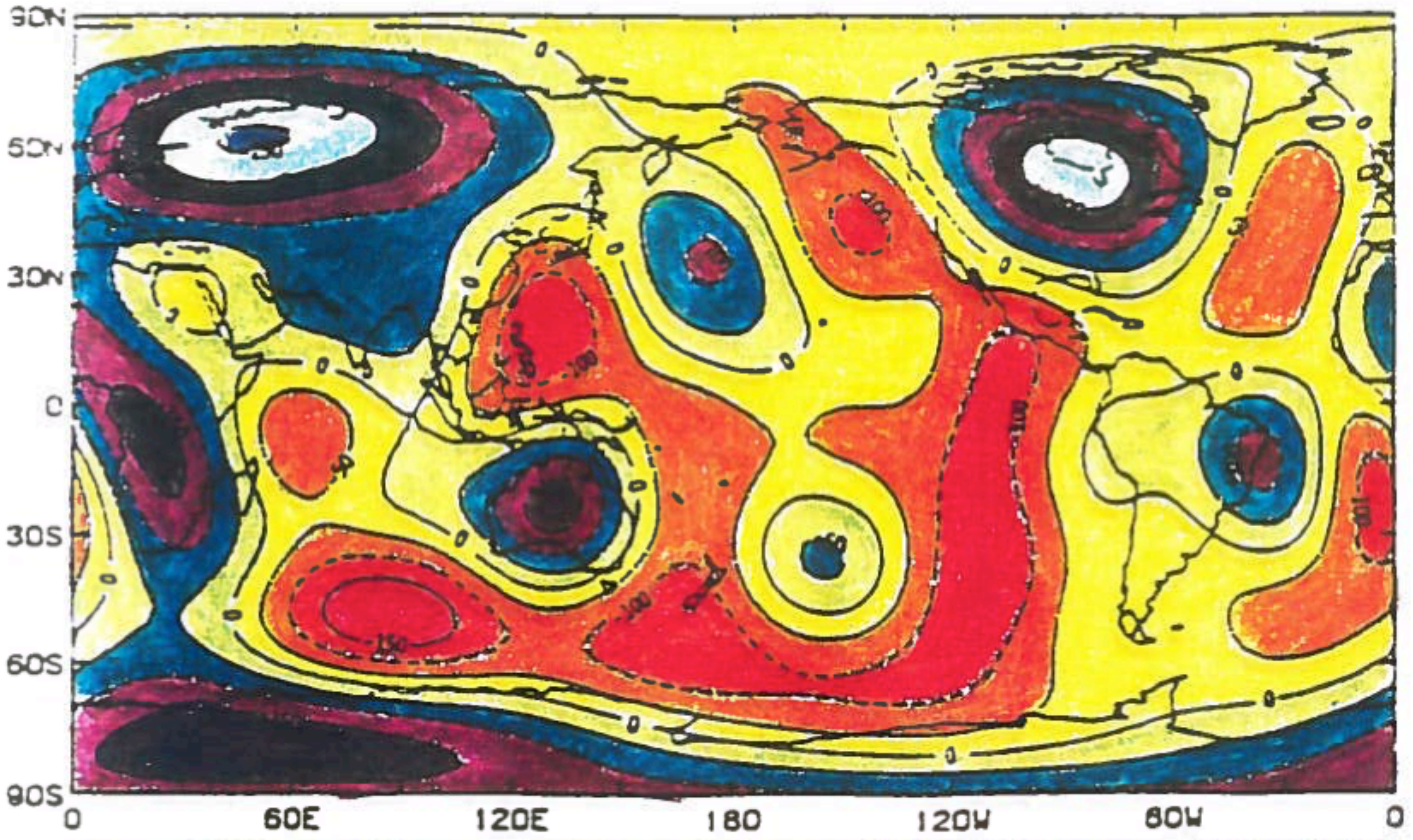

Woodhouse & Dziewonski, 1984

b

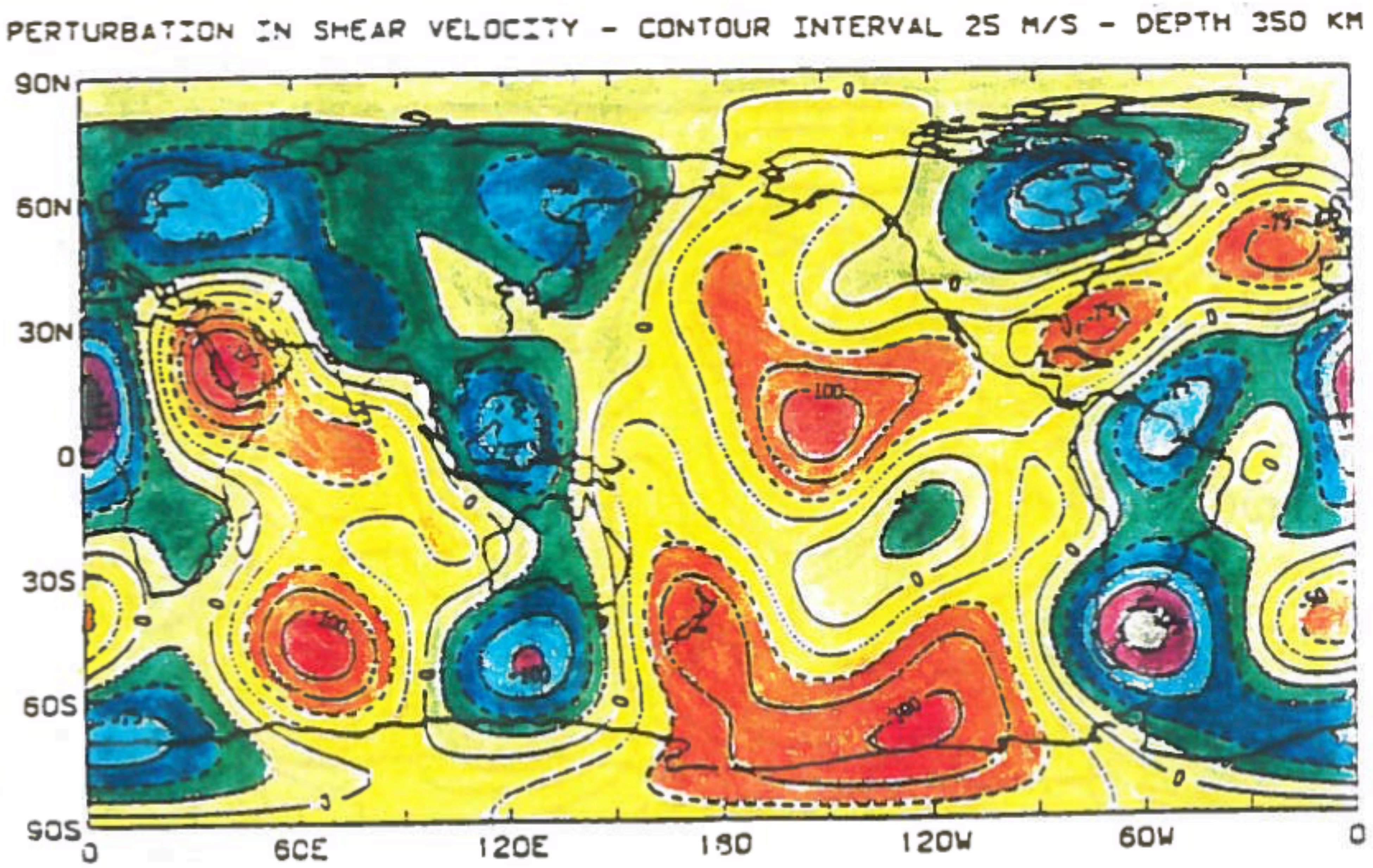

A recent global model of the uppermost mantle

Debayle et al, 2016

from 1,359,470 Rayleigh waves, up to the fifth overtone!

A high-resolution global model revealing slab behaviors

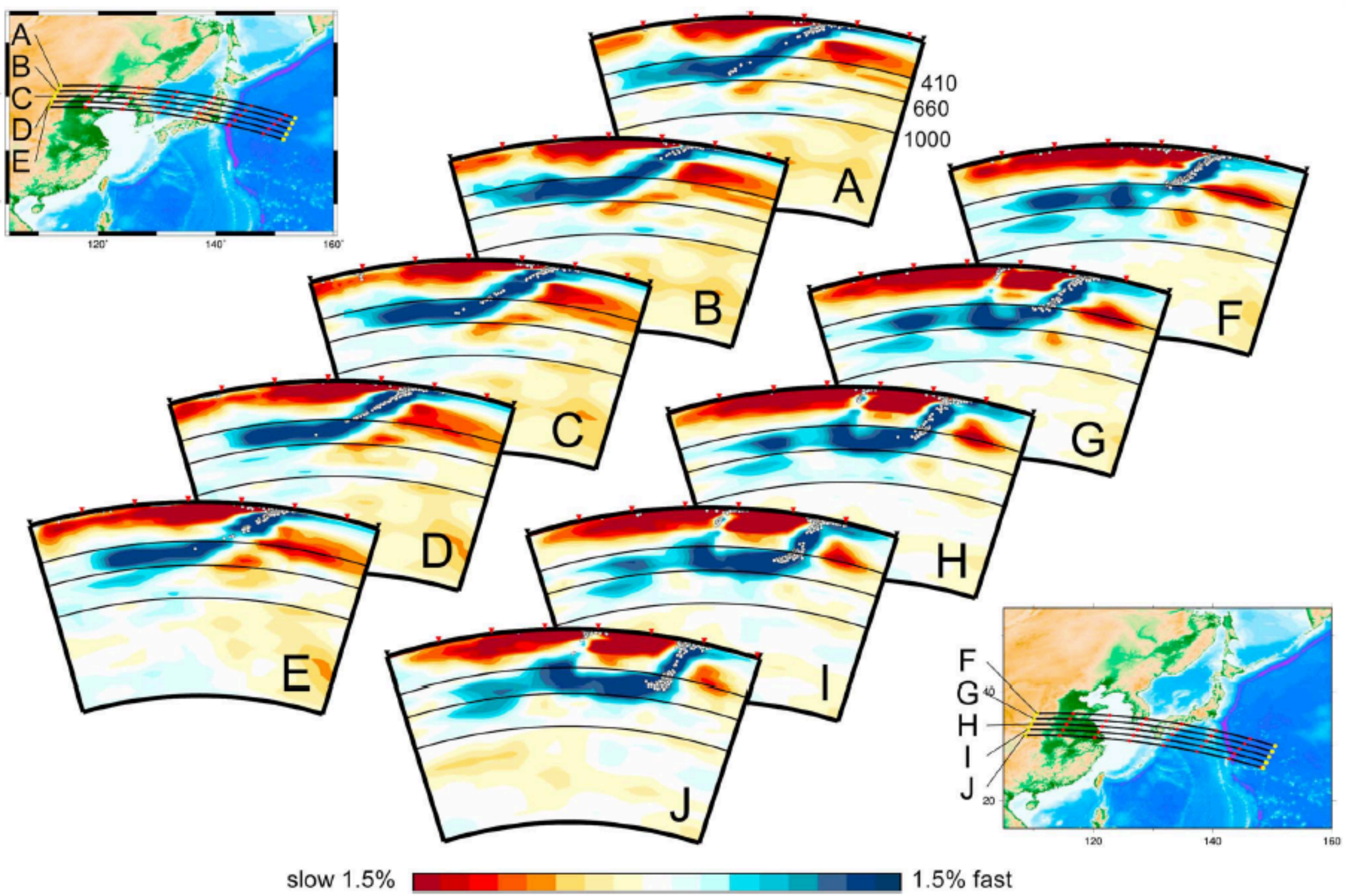

Figure 3. Successive slices of slab images. (top, left) Across the northern Honshu arc along profiles A–E shown in the top left map. (bottom, right) Across the northern Bonin arc along profiles F–J shown in the bottom right map. The color scale is ±1.5% in *P* wave velocity perturbation (blue = positive, red = negative). White dots indicate earthquake hypocenters within a band 50 km wide on both sides

Fukao & Obayashi (2013) conducted the most thorough and impressive survey of subducting slab behaviour, from cross-sections across their high resolution P-wave velocity global model. It was obtained from more than 10 million travel-times, using a finite-frequency extended ray theory.

Fukao & Obayashi, 2013

A high-resolution global model revealing slab behaviors

Their study reveals that many slabs flatten out and stagnate either above or around the 660 km discontinuity, or at depth of about 1000 km. Only a few slabs penetrate deep into the lower mantle.

Fukao & Obayashi, 2013

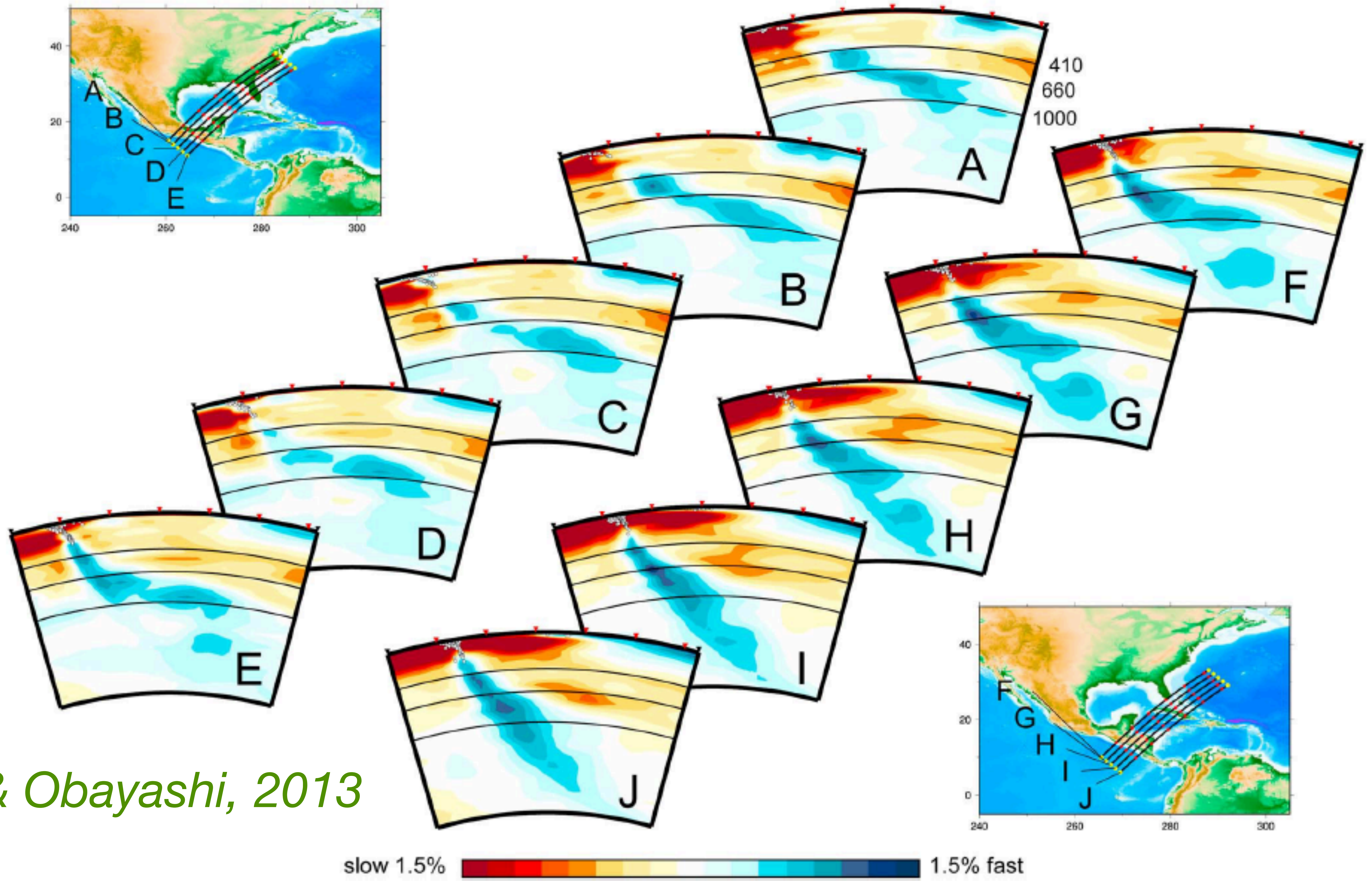

Figure 16. Successive slices of slab images. (top, left) Across the northern part of the Central America arc along profiles A–E shown in the left top map. (bottom, right) Across the middle part of the Central America arc along profiles F–J shown in the right bottom map. Other features are the same as those described in Figure 3.

What about plumes in the lower mantle?

- The resolution of seismic tomography in the lower mantle is not as good as in the upper mantle. Mantle plumes are expected to be rather narrow features (diameter ~100-400 km) with a rather modest temperature excess (~200-400 K), yielding seismic velocity anomalies of ~2-5%.

- Therefore, it seems difficult to image mantle plume conduits in the lower mantle. Nevertheless, several teams have developed tools for addressing this issue. I will present three of them.

Scattering tomography

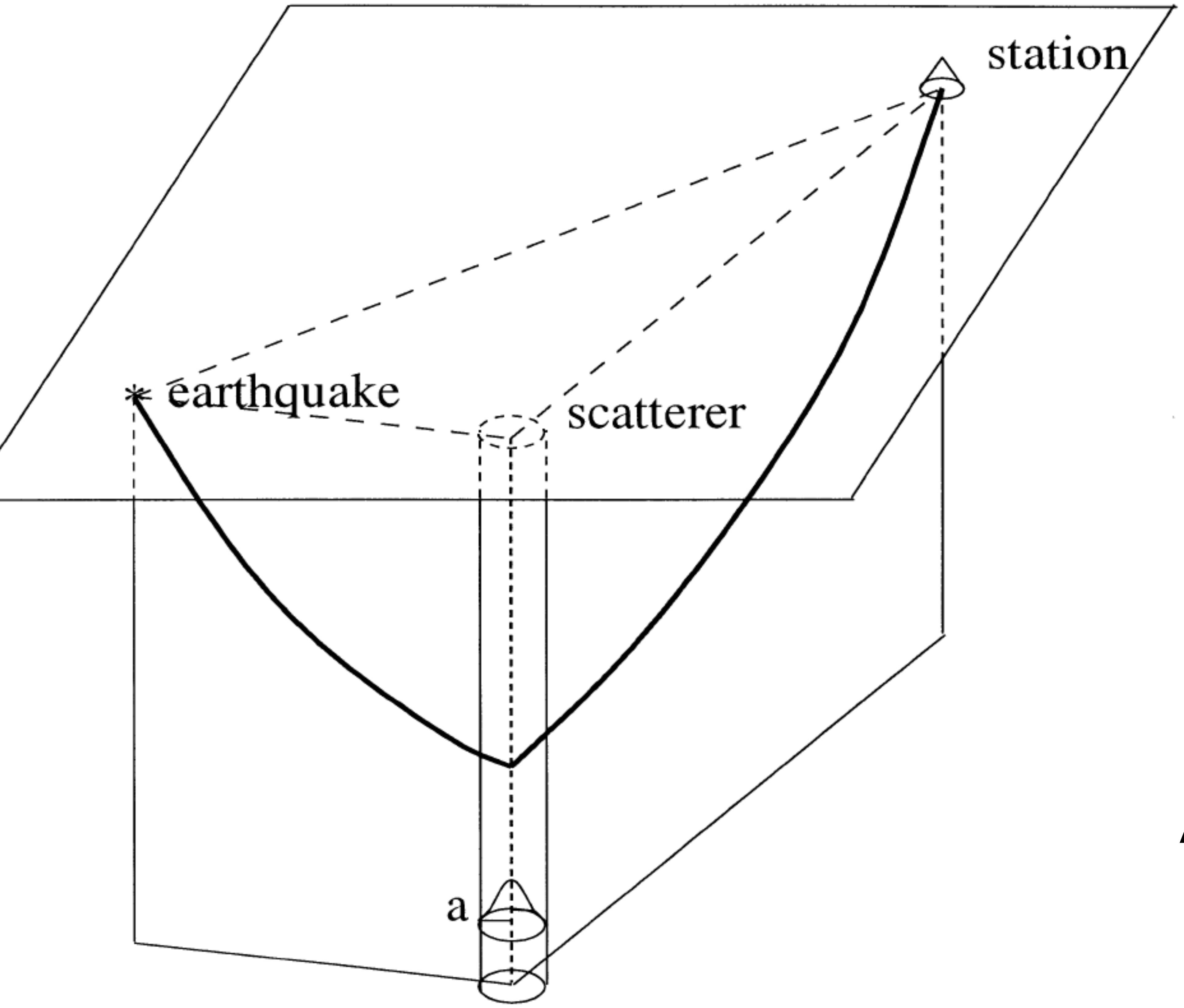

Narrow velocity anomalies scatter seismic waves. Coherent scattering from a vertical structure, such as a plume, can produce a sizable scattered wave. **Scattering tomography** stacks waves that can be scattered from a given location.

A strong slow anomaly was detected that way, north-west of Hawaii.

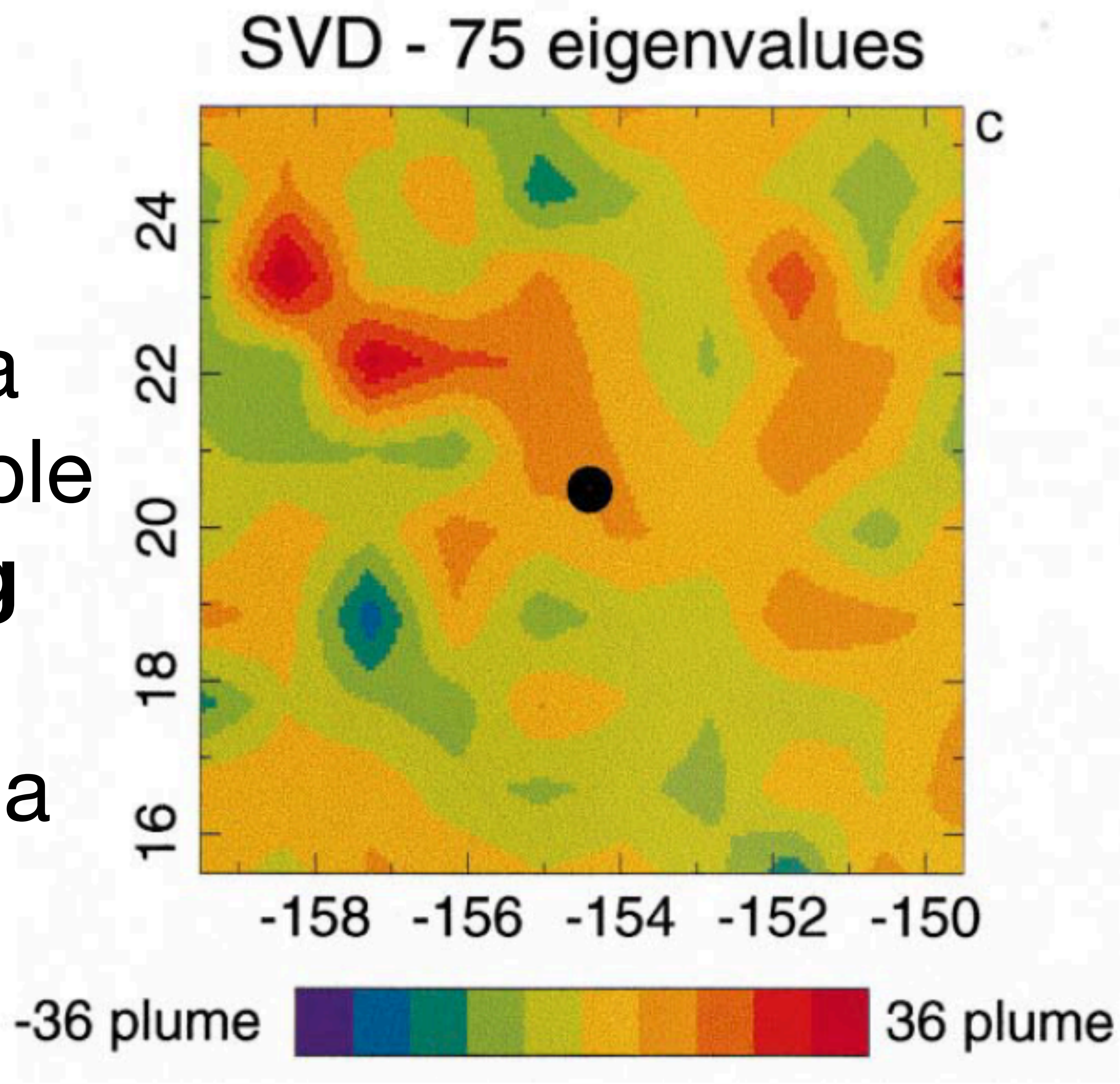

Hawaii

Ji Ying & Nataf, 1998

Finite frequency P-wave tomography

- Wavefronts '*heal*' when travelling in a low-velocity region, thereby smearing out the travel-time anomaly it produces. Montelli et al (2004) used a **finite-frequency** theory, which goes beyond classical ray theory, and produced a global map of the lower mantle. Integrating over the full depth of the lower mantle to emphasize vertical structures such as plumes, they detected several slow anomalies that seem to be related to known hotspots.

- The amplitude of these anomalies is stronger than expected for usual thermal mantle plume models.

Finite frequency P-wave tomography

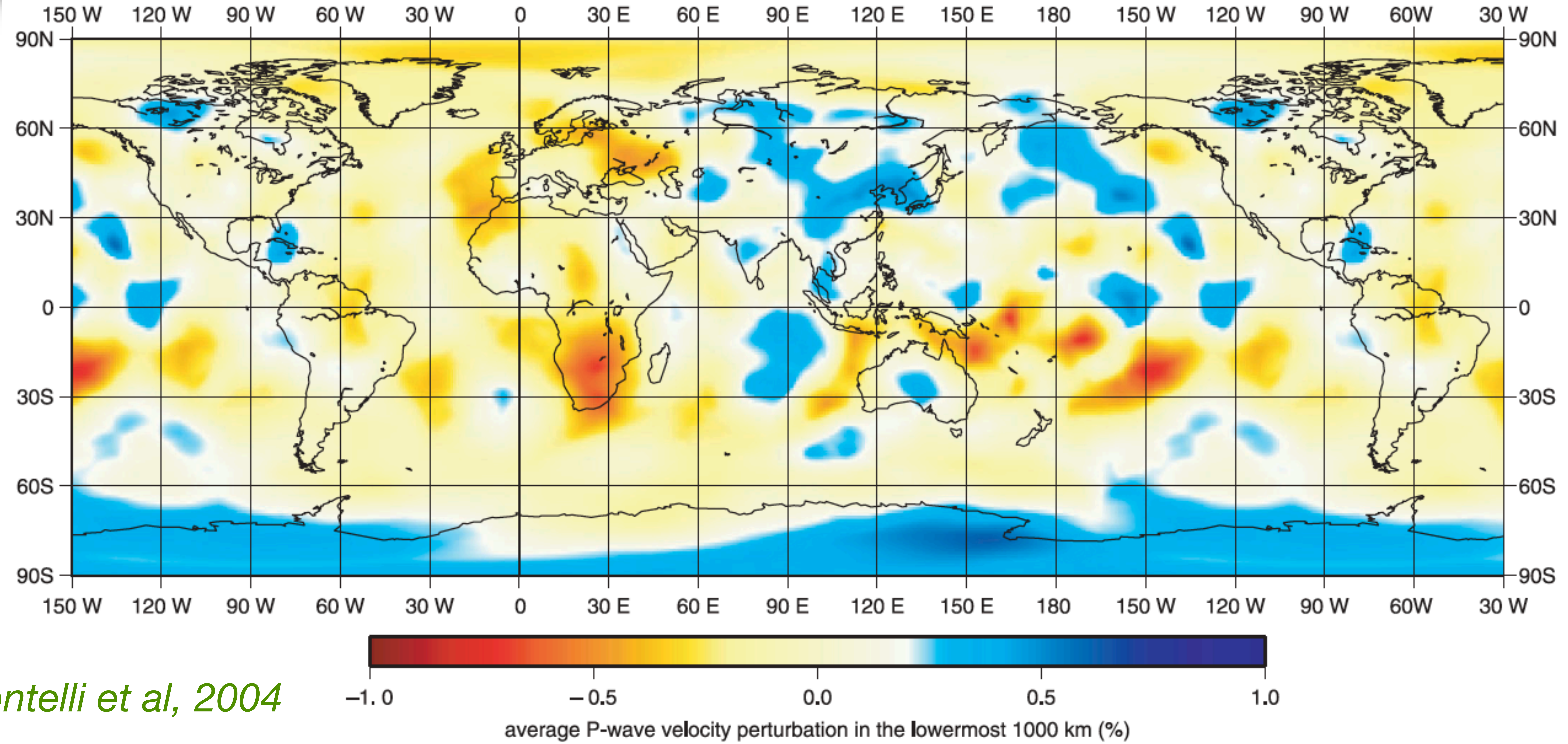

Montelli et al, 2004

Fig. 1. Vertical average over the lowermost 1000 km of the mantle of the relative velocity perturbation $\delta v_p/v_p$. The averaging emphasizes features that are continuous with depth. Map has been wrapped around to have complete views of both the Atlantic and the Pacific oceans.

Finite frequency P-wave tomography

- Wavefronts '*heal*' when travelling in a low-velocity region, thereby smearing out the travel-time anomaly it produces. Montelli et al (2004) used a **finite-frequency** theory, which goes beyond classical ray theory, and produced a global map of the lower mantle. Integrating over the full depth of the lower mantle to emphasize vertical structures such as plumes, they detected several slow anomalies that seem to be related to known hotspots.

- The amplitude of these anomalies is stronger than expected for usual thermal mantle plume models.

Full waveform tomography

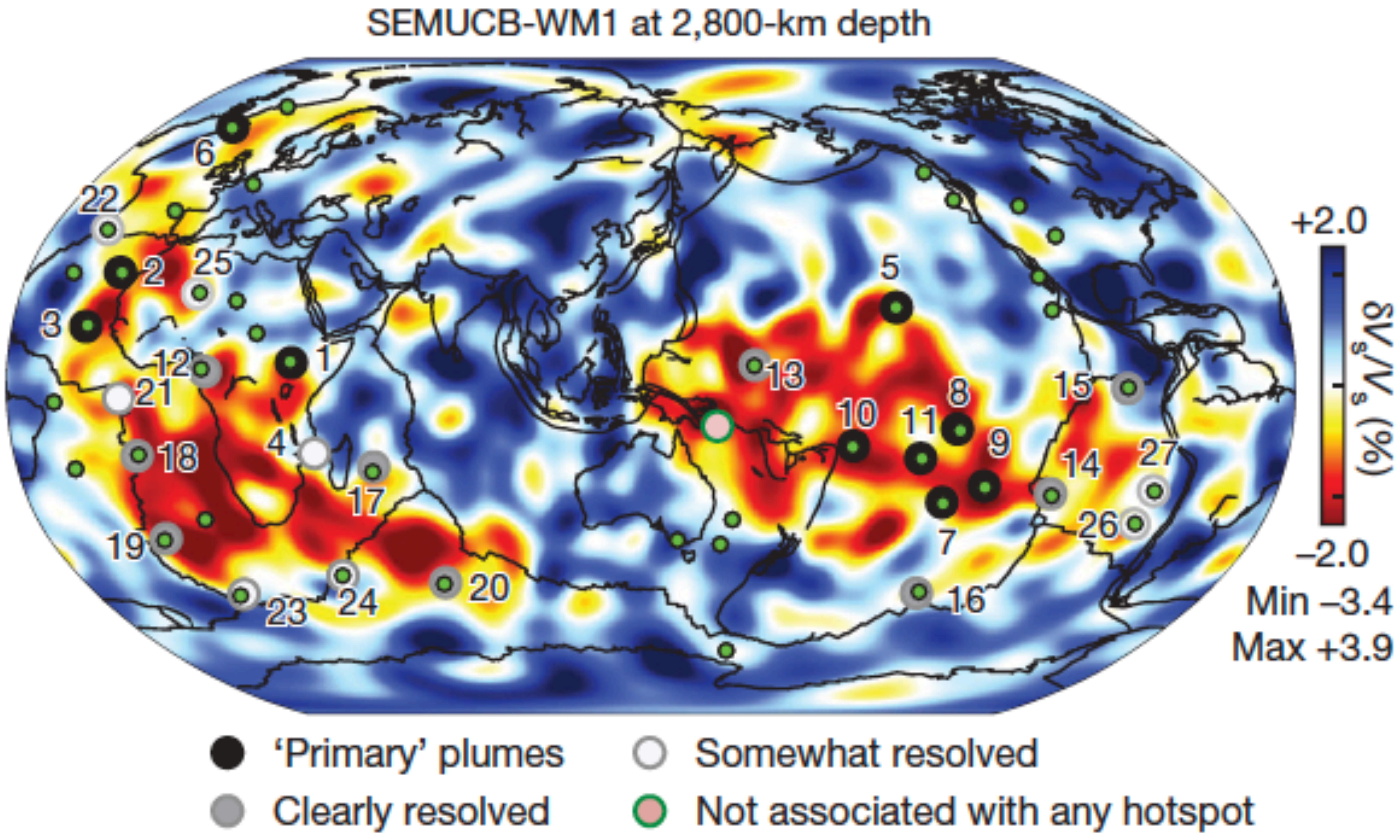

French & Romanowicz, 2015

More recently, French & Romanowicz (2015) produced a global mantle tomographic model, using a method that partly accounts for scattered waves. They find large slow anomalies that correlate with several hotspots.

Full waveform tomography

French & Romanowicz, 2015

Two remarks

1. None of the mantle plume ‘detections’ presented above has yet received a large consensus.

2. All these studies show much larger anomalies than expected for ‘standard’ thermal plumes (another plume paradox!).

2.5. Plate tectonics: where, why and how?

lava lake tectonics

Erta Ale
Ethiopia

© Chris Rowan